EDGE STABILIZED RIBBON GROWTH;

A NEW METHOD FOR THE MANUFACTURE OF PHOTOVOLTAIC SUBSTRATES

by

Emanuel M. Sachs

B.S. Massachusetts Institute of Technology
(1976)

M.S. Massachusetts Institute of Technology
(1976)

Submitted to the Department of
Mechanical Engineering
In Partial Fulfullment of the
Requirements of the
Degree of

DOCTOR OF PHILOSOPHY

at the

MASSACHUSETTS INSTITUTE OF TECHNOLOGY

May, 1983

Signature of Author _____
Department of Mechanical Engineering
May 1983

Certified by _____
Thesis Supervisor

Accepted by _____
Chairman, Ph.D. Committee

Accepted by _____
Chairman, Mechanical Engineering Department Committee

EDGE STABILIZED RIBBON GROWTH;

A NEW METHOD FOR THE MANUFACTURE OF PHOTOVOLTAIC SUBSTRATES

by

Emanuel M. Sachs

Submitted to the Department of Mechanical Engineering
on April 27, 1983 in partial fulfillment of the
requirements for the Degree of Doctor of Philosophy in
Mechanical Engineering

ABSTRACT

A new ribbon growth technique has been developed for the manufacture of semiconductor substrates intended for photovoltaic application (solar cells). In this Edge Stabilized Ribbon (ESR) method, the crystal growth proceeds from the surface of the melt. The edges of the growing ribbon are held in place by capillary attachment to wetted strings which are brought up through the melt and are frozen into the edges of the growing ribbon. The capillary stabilization of the edges allows for growth over a wide melt temperature range of $\pm 10^{\circ}C$.

This direct melt-to-wafer technology is intended to substitute for semiconductor industry technology wherein bulk crystals are laboriously sawed into wafers, while offering a better compromise between ease of manufacture and material quality than current ribbon growth techniques.

Silicon ribbon has been grown in widths of 2.5, 5.6 and 10.0 cm, at growth speed ranging from 2 to 18 cm per minute, with 6 - 7 meters of ribbon resulting from a growth run limited only by the capacity of the crucible. The ribbon thickness is determined by growth speed and ribbon of controlled thicknesses from 5 to 400 microns has been grown. Solar cells fabricated on ESR material have demonstrated 14.0% active area conversion efficiencies on $3.5cm^2$ cells. This is approximately 85% of the efficiency measured on co-processed single crystal control wafers.

The wide latitude in melt temperature allowed during ESR growth results in excellent growth stability with a minimum of operator intervention required. The ESR process is shown to be an excellent candidate for the manufacture of low cost solar cells.

Thesis Supervisor: Dr. David Adler

Title: Professor of Electrical Engineering

TABLE OF CONTENTS

PROJECT SUMMARY, HISTORY AND ACKNOWLEDGEMENTS

The goal of this project is to produce low cost silicon sheet for use as solar cells. Toward this goal, a new crystal growth technique, Edge Stabilized Ribbon (ESR) has been introduced for the continuous manufacture of crystalline silicon ribbon. Specialized equipment has been designed and constructed for the growth of ESR ribbon. Long, wide and thin ribbons have been grown by the ESR technique with excellent growth stability, process repeatability and with a minimum of operator intervention required. The control of ribbon width and thickness is excellent. ESR material has been shown to have good electronic properties, and it has been fabricated into solar cells which consistently demonstrate conversion efficiencies of over 10%. New diagnostic techniques, developed for the characterization of polycrystalline silicon, have demonstrated that the conversion efficiencies are limited only by the density of dislocations in the material, and progress has been made in reducing these dislocation densities with significant improvements in cell efficiencies observed.

This work was started as a doctoral project at the Massachusetts Institute of Technology, and this document is the culmination of the research envisioned for this thesis. However, as a result of the significant accomplishments and promise of the ESR technique, this work will continue actively with the intent of near term commercial application of this technology to the photovoltaic generation of power.

A fellowship from the Fannie and John Hertz Foundation provided the necessary framework and support to initiate and undertake this work. The initial demonstration experiments, the growth of tin ribbon, were conducted in the Institute Crystal Growth Facility. Early results were sufficiently promising to prompt the filing of a patent application.

At this stage, broader support was needed to continue the work, and an agreement was reached with the Invention Management Group at Arthur D. Little, Inc., of Cambridge, Massachusetts to provide for continued research support at their facility and to provide for commercialization of the technology at the appropriate time.

With the help of the Arthur D. Little support, ESR growth of silicon ribbon was demonstrated (2.5 cm wide). Work continued as essentially a one man technical effort for approximately one and one half years until a contract was arranged with the Solar Energy Research Institute (SERI) of the Department of Energy. This contract was cost shared by ADL and provided the support to considerably expand the project.

At the initiative of the Physical Systems Research Section of ADL, a new lab was constructed to undertake the research on ESR. The SERI funding provided for the construction of a new growth furnace and allowed for the growth of 10 cm wide ESR ribbon, and for the fabrication and characterization of solar cells as discussed later.

The project is currently in its second year of SERI funding cost shared by ADL and is very much an ongoing and promising concern.

The author wishes to thank the Hertz Foundation for its continued support and good wishes concerning this work. The freedom provided by their support was a vital factor throughout.

Also vital is the support of the Arthur D. Little Invention Management Group and especially Mssrs. Samuel Tishler and Walter Cairns for their continuing faith in the prospects of the photovoltaic industry.

The research contracts with SERI have been indispensible in allowing for the accelerated development of the ESR process and its approach to commercialization.

Thank-you to the staff of the MIT Crystal Growth Facility, especially to Mr. Arthur Linz and Dr. David Gabbe.

Many thank yous go to members of the staff at ADL who have contributed to this work before and especially during the SERI contracts. Continuing thanks to Ms. Debra French, Mr. Douglas J. Ely, Mr. Russell Smallman, Dr. Edward Peters, and Dr. Mehmet Rona. Thank-you to Dr. Edward J. Cook whose quick recognition of the potential of ESR made ADL support possible.

The support and interest of Prof. Thomas Bligh are much appreciated. His perspectives were a valuable source of balance in this work.

Thank-you to my parents, Adele and Moshe Sachs, for their constant support and encouragement.

Daily thank-you to my wife, Dr. Carol Takvorian for understanding, accommodating and supporting a demanding lifestyle.

Profound gratitude to Dr. Thomas Surek, who as colleague and mentor at Mobil Tyco Solar Energy Co. taught me crystal growth and who, as friend, has continued to help with advice and enthusiasm.

Special thank-you to Prof. David Adler who undertook to guide this work and who was instrumental in its initiation. His special quiet enthusiam and dedication to teaching have provided motivation through many difficult periods.

Thank-you to Prof. Woodie Flowers, who has always understood the intent and motivation of this work and has helped to keep it on track toward completion. This work has allowed for the extension of a valued and priviledged relationship between student, teacher and friend for which the author is most grateful.

CHAPTER 1

BACKGROUND

1.1 The Potential of Photovoltaics

Photovoltaics, the direct conversion of sunlight to electricity by solar cells, is a demonstrated and attractive "alternative energy" technology. The potential contribution of photovoltaics may be understood by noting that the solar power incident on the contiguous 48 states of the U.S. averaged over a yearly cycle is approximately 1.47×10^{15} watts[1]. This is approximately 500 times the power consumption of the U.S. including electricity, heat, transportation, and other uses, averaged over a yearly cycle.

Economists may better understand the potential by realizing that if commonly accepted near term pricing goals of $0.70 per peak watt of photovoltaic generating capacity are attained, such systems would have a payback period of 7-10 years when competing with utility purchased power at $.07/per kilowatt-hour. The systems are expected to have a service life of over twenty years.

Current pricing levels are approximately one order of magnitude above these near term goals. This is the primary factor which prevents photovoltaics from playing anything but an incidental role in power generation. These economic considerations are so severe as to put the goals beyond the reach of mere refinements of current technologies, but rather call for major new innovation in all areas of fabrication; hence, the impetus for this work.

1.2 The Constitution and Function of a Solar Cell

Light photons incident on a semiconductor material are capable of breaking the covalent bonds which bind the valence electrons to atoms thereby liberating the electron. This process also results in the formation of a mobile "hole", which is just the absence of an electron from a covalent bond. The energy required to break a covalent bond, and therefore the minimum photon energy required to create a free electron-hole pair is called the band gap, which is a fundamental property of the material.

If the electron and hole are not separated, they will quickly recombine, not having a chance to contribute to a net current flow. To separate the charge carriers, an energy barrier or junction is fabricated into a solar cell which provides a built in internal electric field. This field acts to segregate the photogenerated carriers, as electrons and holes move in opposite directions under the influence of an electric field. The field is created by an abrupt junction between two regions, one rich in holes (p-type) and the other rich in electrons (n-type). These regions consist of material in which some of the host atoms in the lattice have been replaced by selected impurity or dopant atoms. The transition region between the two types of material is called the p-n junction.

A schematic drawing of a solar cell is presented in Figure 1. The starting material in the fabrication of the cell is the semiconductor wafer which is lightly and uniformly doped, in this case, p-type. The p-n junction is then fabricated by diffusing (or other means) in n-type

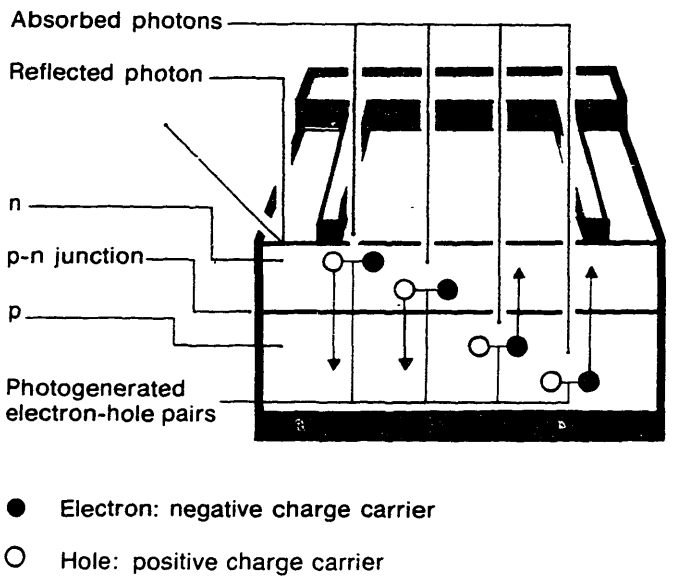

Figure 1. Construction and function of a solar cell.[2]

dopant atoms resulting in a heavy concentration confined to a shallow region near the wafer surface. The n-type dopant atoms overcompensate the native p-type material in this region resulting in an n-type layer and a p-n junction. Metal contacts or electrodes are provided on the top and bottom of the cell, with the top contact formed in fingers to allow the light to hit the semiconductor material. An anti-reflection coating (not shown) is added to minimize losses due to reflection of light from the surface of the cell.

In operation, with light falling on it, a solar cell normally functions between two extreme cases. The first extreme is to directly connect the top and bottom contacts of the cell and create the short circuit condition, where no voltage is present across the cell. In this case a photogenerated current will flow external to the cell. This short circuit current will be roughly proportional to the intensity of incident light, for a constant incident spectral distribution. The second extreme is the open circuit condition in which no external current may flow. In this case, the internal photogenerated current causes a reduction in the height of the barrier at the junction, and results in a voltage which may be measured external to the cell, the open circuit voltage. The open circuit voltage also increases with increased incident light intensity, but here the dependence is very weak. Rather, the open circuit voltage is related to the band gap of the semiconductor used, and is equal to roughly one half the band gap. For example, silicon has a band gap of 1.1 electron volts, and silicon cells typically deliver 0.55 volts in open circuit conditions.

In both these extreme cases, the solar cell is delivering no power. In a useful situation, therefore, a solar cell is connected to a properly matched resistive load. In this case, the cell operates between the extremes of short circuit and open circuit and the cell delivers power to the external load. Typically, a cell might deliver 85% of the short circuit current at 85% of the open circuit voltage.

The conversion efficiency of a solar cell could approach 100% if the incident light were monochromatic with a photon energy just slightly larger than the band gap. In practice, the maximum possible efficiency is considerably lower as determined by the band gap of the material and the spectral content of sunlight. Solar photons with energies lower than the band gap (long wavelengths) cannot produce electron hole pairs and therefore create no photogenerated current. At the same time, since a single photon can create only one electron hole pair, any photon energy in excess of the band gap can only produce heat within the crystal.

For a given spectral distribution, there is a particular value of band gap which minimizes the losses and results in the highest potential cell efficiency. For sunlight, this value of band gap is approximately 1.45eV resulting in a maximum efficiency of roughly 26%. Silicon, the material of concern in this work, has a band gap of 1.1eV and a maximum efficiency of roughly 22%, at $20^{o}C$.[2]

Stacking cells with different bandgaps can result in higher efficiencies, and silicon has the ideal band gap for the bottom cell of a two-stack "tandem" cell.[3] However, such advanced concepts are not yet of practical value, and are not treated in this work.

From a practical standpoint, the conversion efficiency is largely determined by the "diffusion length" of photogenerated charged carriers. The diffusion length measures how far carriers can move in the wafer before suffering "recombination", or rebinding to a stationary atomic site. A long diffusion length allows for carriers generated deep within the wafer to reach the junction and do useful work, and therefore leads to higher conversion efficiencies. Diffusion length is limited by all manner of crystal imperfections includig: impurity atoms, dislocations, and grain boundaries. Thus, the highest efficiency is expected from dislocation free perfect single crystal substrates.

1.3 Materials for Photovoltaics

A broad range of semiconducting materials is now under investigation for use in solar cells. These include crystalline silicon, amorphous silicon, gallium arsenide, cadmium telluride, copper sulfide, copper indium diselenide and many others. These materials span a tremendous range in material properties, including optical absorption properties and band gap.

While all the materials mentioned above have potential for low cost photovoltaics, crystalline silicon is the material most commonly used in solar cells today. The abundance of the material, an established technology base borrowed from the semiconductor industry and a good match of properties (energy band gap) to the solar spectrum make silicon the logical choice. Additionally, silicon solar cells have been found to be extremely tolerant of crystallographic imperfections with greater than 10% efficient cells routinely fabricated on highly polycrystalline and imperfect substrates. In fact, once the grains exceed approximately 1 - 3 mm in extent, grain size is usually not the limiting factor in cell performance.[4] For all these reasons, the present work concerns the production of silicon substrates.

1.4 The Cost of Silicon Solar Cells

At present, the single largest cost component in the manufacture of a solar cell is the silicon wafer itself. In fact, the wafer accounts for over half the total cost of a panel with the remaining costs distributed over junction formation, contact application, anti-reflection coating, interconnection, and encapsulation.

High wafer costs result from expensive manufacturing methods, coupled with the inefficient use of expensive semiconductor-grade raw silicon. The efficiency of a silicon solar cell is maximized with a wafer thickness of 60 - 100 microns.[5] However, current methods produce much thicker wafers, as discussed in Chapter 2.

Therefore, the present work is directed at the development of a new manufacturing method for the production of thin wafers or substrate. Accordingly, this work addresses other fabrication steps only in the context of testing and qualifying the substrate produced.

1.5 The Performance of Silicon Solar Cells

Solar cells are most commonly rated at peak solar flux or "air mass 1" (AM1), which correspond to 1000W/cm^2 of solar radiation.* The theoretical upper limit to the conversion efficiency of silicon solar cells at AM1 (as determined principally by the band gap) is approximately 22%.[5] Single crystal substrates can be fairly reliably fabricated into 15% efficient solar cells.

It is generally accepted that the minimum efficiency required for silicon solar cells to be economical is 10%. Thus, a 10% efficient panel of area 1m^2 will deliver 100 watts of electrical power at peak solar flux corresponding to AM1 conditions.

Solar cells tend to be low voltage, high current devices, a fact which significantly impacts their design. For example, a 10% efficient silicon cell of 100 cm^2 area will deliver 1 watt of electrical power at AM1 conditions at approximately 0.5 volts and 2.0 amps. Of course, cells may be series-parallel connected to deliver substantially any voltage, current combination.

---

*Air Mass 1 is the designation given to peak solar flux reaching the ground at sea level. The name derives from the approximately 1 mile of atmosphere penetrated by the sun when directly overhead. Air Mass 0 refers to solar intensities encountered in space bound application.

CHAPTER 2

SUBSTRATE MANUFACTURING TECHNIQUES

2.1 Introduction

The various methods for the production of silicon substrates are discussed in this Chapter. These include ingot technologies which require a sawing step to produce wafers, and sheet growth methods where thin ribbon is produced directly and no sawing is required. The fundamentals of ESR growth are introduced.

All these methods begin by melting semiconductor-grade "polycrystalline" silicon, an extremely pure form of silicon. While silicon is abundant, and metallurgical-grade silicon is inexpensive, the highly purified material needed for semiconductor applications is quite expensive. Current costs vary between 50 and 100 $/kg. Therefore, the efficient utilization of raw material is critical to economical wafer production. As discussed below, this is one of the critical factors mitigating against ingot methods and one of the most important benefits of ESR growth.

2.2 Traditional Manufacturing Methods (Ingot Technology)

At present, most solar cell wafers are produced by the Czochralski crystal growth technique; the technique used to grow the majority of wafers used by the microelectronics industry. Figure 2 presents a schematic drawing of this technique wherein a cylindrical boule, or ingot

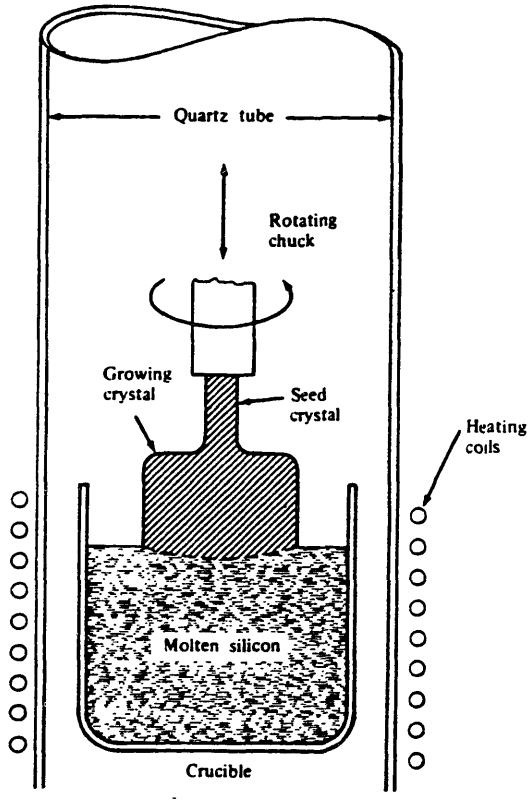

Figure 2. Schematic drawing of Czochralski growth.[6]

often of single crystal character, is grown directly from the melt surface. Following growth, the crystal must be sliced by one of several expensive and laborious techniques. The difficulty of the slicing process is due to the fact that silicon is an extremely hard and brittle material. The slicing difficulty further leads to inefficient raw materials utilization as large wafers may be sliced no thinner than 400 microns with an attendant saw kerf loss of 400 microns. This total per slice thickness of 800 microns compares poorly with the optimal cell thickness of 60-100 microns.

Another major disadvantage of Czochralski growth is that the round wafers produced must either be cut into squares or result in poor packing densities in panels, with a resultant loss in overall panel efficiency.

Alternative ingot technologies involve casting large rectangular blocks of polycrystalline silicon, bypassing the slow Czochralski crystal growth step. Nonetheless, these ingots must be sliced into wafers, with the associated high costs and poor material utilization. Therefore, casting methods are only slightly more economical than Czochralski growth.

Due to the difficulty of crystal growth and cutting processes, as well as the poor utilization of raw material, wafer costs are high - at least an order of magnitude too high for photovoltaic purposes.

2.3 Sheet Growth Technologies

An alternative approach to ingot growth which obviates the need for expensive cutting is shaped crystal growth where a thin flat crystalline ribbon is grown directly from the melt. Such an approach has the potential to eliminate both cutting and surface preparation steps as solar cells may be fabricated directly on the surface as grown.

Figure 3 and 4 show schematic illustrations of the two most widely known ribbon growth methods. In Edge-Defined-Film-Fed-Growth (EFG), the "die" is immersed in a pool of molten silicon. The die is made of a material wetted by silicon graphite being the most often used material. The liquid flows up the center slot by capillarity and is contacted at the top with a seed. Upward pulling results in the continuous solidification of melt at the interface and the growth of a ribbon.[7,8]

In Web-Dendritic growth, the growth proceeds directly from the surface of the melt with no foreign matter present. The edges of the ribbon are held in place by the propogation of dendrites into a supercooled melt, below the free melt surface. These dendrites then act to hold the ribbon defining meniscus in position by capillary attachment, thus preventing the collapse of the growing ribbon into a small cylindrical boule, similar to Czochralski.[9]

As summarized in Figure 3 and 4, there are four principle areas of difficulty associated with these techniques; mechanism of edge-definition, the degree of temperature control required, the thickness control realizable, and the ability of the process to reject impurities back into the melt. The first three taken together may

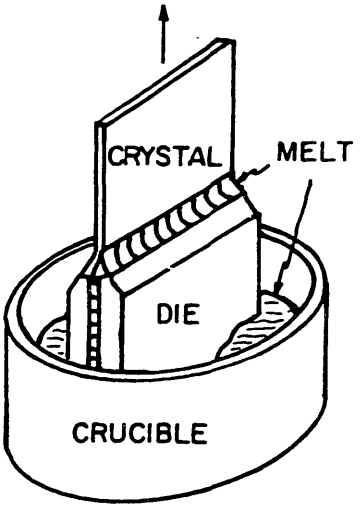

Impurity segregation:	No
Melt temp. control:	$\pm$ 1.0°C
Typical thickness:	350μ
Width control:	Thermal

Figure 3. Schematic of Edge Defined Film Fed Growth (EFG).[10]

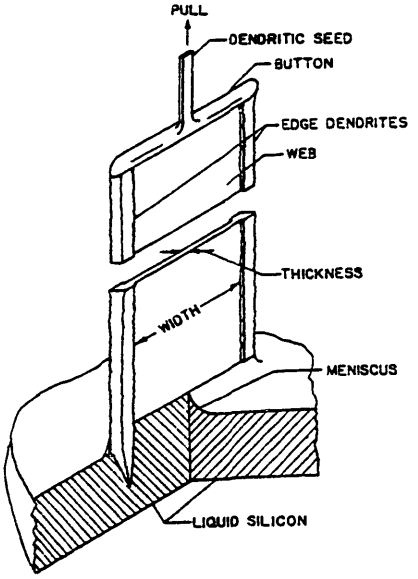

Impurity segregation:	Yes
Melt temp. control:	$\pm$ 0.1°C
Typical thickness:	150μ
Width control:	Thermal

Figure 4. Schematic of Web-Dendritic growth.[11]

generally be referred to as factors influencing growth stability and reproducability. It is important to note that surface tension forces tend to result in the collapse of a growing ribbon into a cylindrical boule, and that any ribbon growth process must somehow, therefore, effect edge stabilization. In the EFG process this stabilization is primarily due to thermal effects with capillary effects playing a relatively small role. As such, the temperature distribution across the die becomes a critical matter requiring the maintenance of temperatures to approximately $\pm$ 1° accuracy at the operating temperature of 1400°C. In Web-Dendritic growth, the edge stabilization mechanism is in fact exclusively thermal in nature because a delicate heat balance condition must be maintained in order to accomplish dendritic growth into a supercooled melt. Such growth requires even more stringent temperature control than does EFG, typically $\pm$ 0.1°C. The stringent temperature control required in either of these processes is one of the primary ingredients contributing to the lack of stability in these processes and the resultant difficulty in their practice.[12]

Some measure of the quality of the resulting material must, of course, be considered in parallel with the ease of manufacturing associated with each method. The Web-Dendritic process produces fairly high quality, single crystal solar cell substrates. In part this high quality is due to the fact that the impurities segregated at the interface as in any directional solidification process are free to find their way back into the bulk of the melt and thereby avoid incorporation into the growing ribbon. Thus, the Web-Dendritic process accomplishes

some purification of the material in the melt.[13] Although the material quality is good, the difficulty of performing Web-Dendritic Growth keeps it from occupying a more prominant position in photovoltaics. By direct contrast, the EFG method grows polycrystalline ribbon of significantly lower quality, in part the lower quality is due to the fact that in the EFG process, segregation of impurities into the melt is impossible because liquid is constantly flowing up the die. The formation and attachment to the growing ribbon of silicon carbide particles from the die is a further severe problem in the EFG technique.[14]

In another class of sheet growth processes, a partially wetted substrate is passed through a melt and coated on one or both sides.[15,16,17] These methods are relatively easy to perform, however, they produce material of inferior quality as there is a great deal of substrate area to contaminate the melt, and any reasonably priced substrate is of questionable chemical content. Further, the close proximity of the substrate to the growth interface leads to a small grain size and poor structure.

In summary, the currently available ribbon growth techniques are not likely to result in significant solar cell cost reduction, as they fail to strike the necessary balance between the quality of the material and the ease with which it may be produced.

2.4 Edge Stabilized Ribbon (ESR) Growth

A successful ribbon growth technique must produce material of photovoltaic quality approaching that of single crystal substrates with a manufacturing ease and growth stability far exceeding that of any currently available technique. In accordance with these goals, this work proposes to establish the Edge Stabilized Ribbon (ESR) growth process.

A schematic illustration of the ESR growth process is presented in Figure 5. In this process the ribbon is grown directly from the surface of the melt and the edges of the ribbon are stablized by strings which pass up through the melt and are frozen directly into the growing ribbon. The edge positions of the ribbon are now controlled exclusively by capillary action as the meniscus is bounded on the bottom by the melt itself, on the top by the growth interface, and at the two edges by capillary attachment to the wetted strings. As thermal effects no longer play any role in determining the edge position of the ribbon, temperature control requirements may be significantly relaxed as compared with other ribbon growth processes. Loosening of the temperature control requirements results in excellent growth stability and allows for the growth of thin ribbon with extremely good thickness control. Finally, growth from the melt surface allows for rejection of segregated impurities into the bulk of the melt, thereby taking advantage of the purification due to directional solidification and allowing for the use of lower grade starting material.

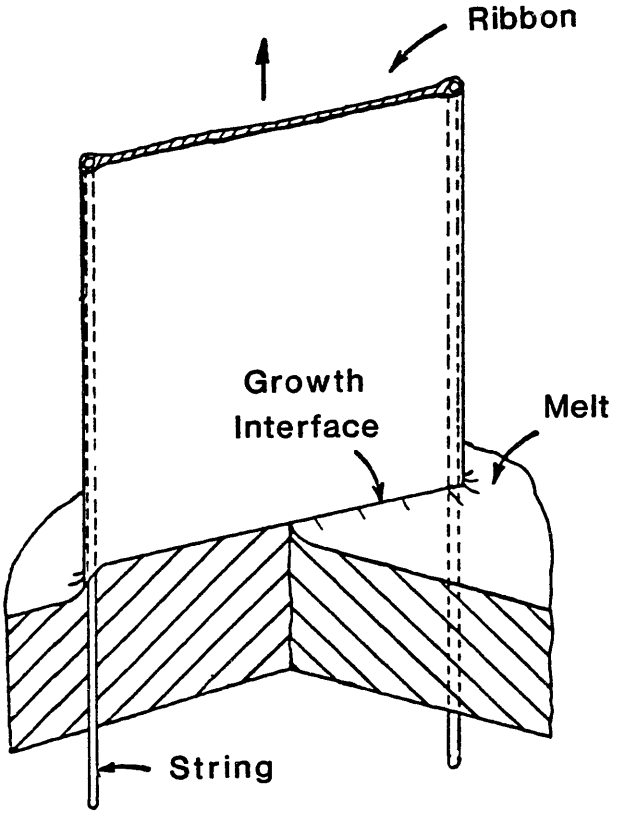

Impurity segregation:	Yes
Melt temp. control:	$\pm 10.0^{\circ}C$
Typical thickness:	50-100μ
Width control:	capillary

Figure 5. Schematic of Edge Stabilized Ribbon growth (ESR).

CHAPTER 3

ESR GROWTH - RESULTS

3.1 Introduction

This work is comprised principally of the growth of low cost silicon ribbon by the ESR technique and the fabrication of high efficiency solar cells on this material. This chapter discusses the progress made and the results achieved in ESR growth, with special attention to the physical characteristics of the ribbon produced, including width, thickness, length, flatness and grain size. Subsequent chapters discuss the apparatus designed and built for ESR growth, the nature of the thermal stress problem which controls ribbon flatness, the fabrication and testing of solar cells made on ESR material, and theoretical aspects of ESR growth. Details of testng methods, including novel techniques are presented in the appendices.

The demonstration and development of ESR growth has taken place in three principal phases:

1. The demonstration of the concept by growing ribbon of tin and a model material (See Appendix A for details).
2. The growth of 2.5 cm wide silicon ribbon in a converted furnace.
3. The growth of 5.6 and 10.0 cm wide silicon ribbon in a specially designed furnace.

The rate of progress on ESR growth has been exceedingly rapid and all development milestones have been met. The achievement of 10.0 cm

width, 50 - 100 micron thickness and growth of up to seven meters per run indicate a process nearing readiness as a low cost production technology.

3.2 Width, Thickness and Length

A multiple purpose crystal growth furnace was retrofitted with specially designed pulling heads and a graphite hotzone for the growth of 2.5 cm wide ESR silicon ribbon. Figure 6 shows a photograph taken through the main viewport of the furnace during growth of 2.5 cm wide ribbon along with a schematic description of the photograph.

Over the course of some 32 growth runs, silicon ribbon was grown under a variety of conditions. Almost all growth runs resulted in total draining of the crucible and the production of approximately six meters of ribbon. A roller puller allowed for the continuous growth of ribbon with lengths of three meters or more grown with little or no interference with the controls.

Ribbon thickness is controlled by the pulling speed (see chapter for details). Typically, a growth speed of 6 cm/min results in ribbon thickness of 50 microns, while a speed of 3 cm/min results in 200 micron thick ribbon. Ribbon grown over a speed range of 2 - 18 cm/minute, resulting in ribbon thickness ranging from 400. to 5 microns, respectively. Figure 7 shows a photograph of a 5 micron thick ribbon sample illustrating the transparency of the sample to visible light. Silicon this thin is not of photovoltaic value, but it serves to demonstrate the capacity of ESR to produce thin material.

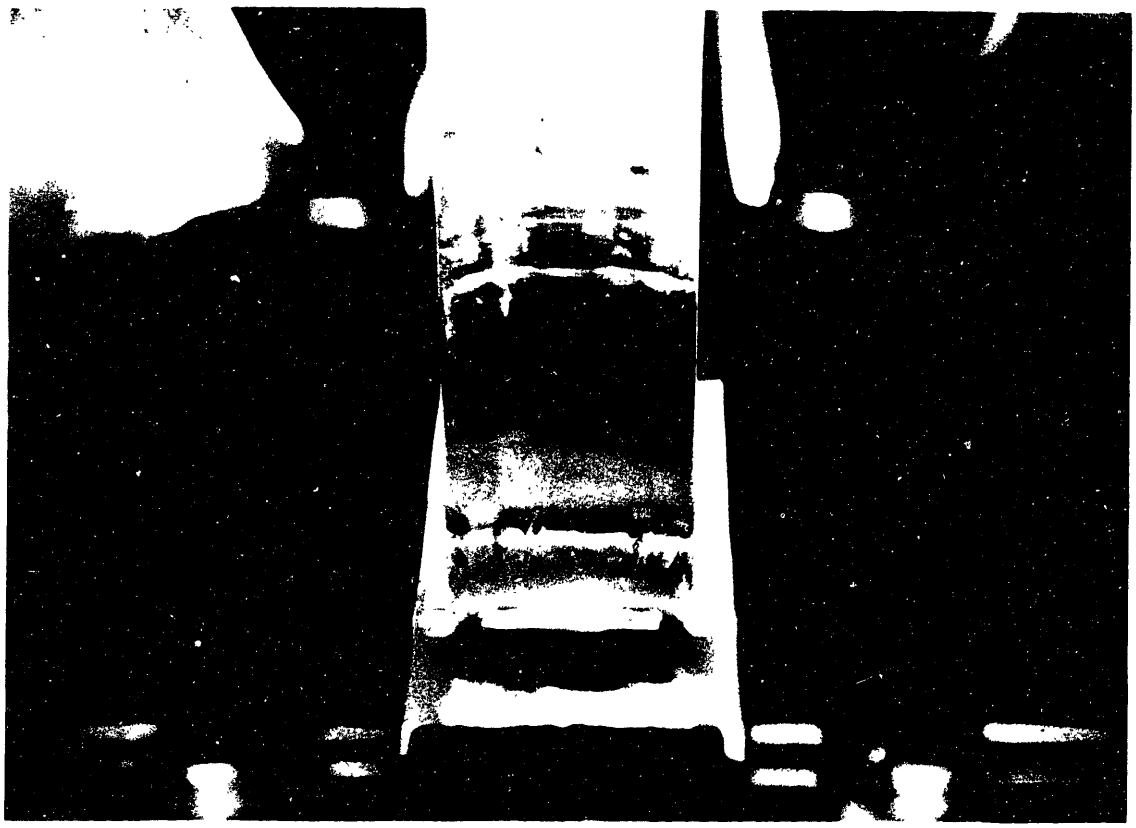

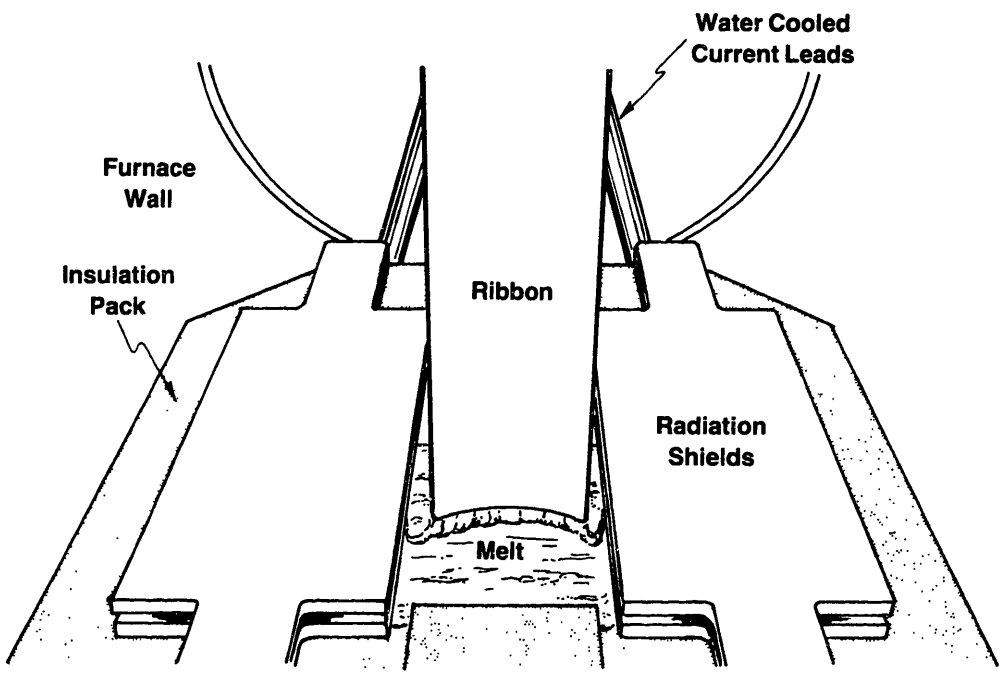

Figure 6. Photograph through main viewport during growth of 2.5 cm wide ESR silicon ribbon. Drawing below details photograph.

The growth of ribbon in the thickness range of 50 - 100 microns is standard operating procedure in 2.5 cm wide ESR ribbon. This thickness range is of great commercial interest as the conversion efficiency of a cell is maximized in this range and the utilization of expensive raw material is minimized. This material offers further advantages of pliability and improved handling characteristics (see Fig. 14 Chapter 5).

Wider silicon ribbon has been grown in a furnace specially designed for ESR ribbon growth. In six growth runs, this furnace has produced 5.6 cm and 10.0 cm wide silicon in 0.5 meter lengths. Figure 8 shows a photograph of 5.6 and 10.0 cm wide ribbon. The ribbon length has been limited by the length of the stroke puller used to pull the ribbon as it has not been flat enough to pass through a roller puller. Total ribbon lengths of 6-7 meters have been produced during a single growth run, made up of combinations of 5.6 and 10.0 cm widths, as both may be grown during the same run.

More recently, flatter material has been grown, in part due to thermal stress reduction efforts, and the furnace will be fitted with a roller puller for continuous growth of ribbon.

The thickness speed relationship for 5.6 and 10 has been found to be similar to that observed for 2.5 cm wide ribbon. Ribbon as thin as 100 microns has been grown in both 5.6 and 10.0 cm widths.

3.3 Growth Stability and Control

Perhaps the most consistent and remarkable feature of ESR has been the ease and reliability of the growth. Growth is almost always initiated at the first seeding with a minimum of the attention usually mandated by crystal growth processes. The growth has been extremely

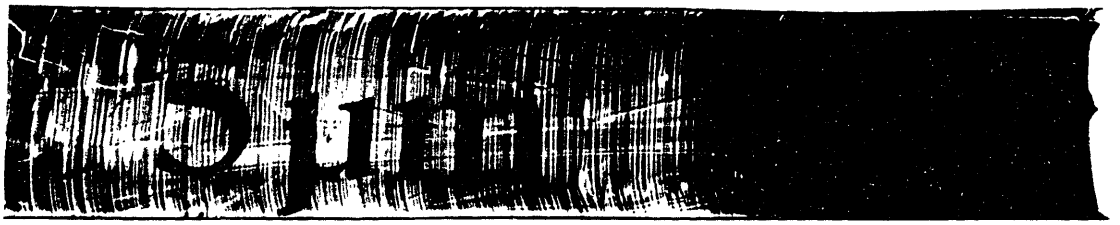

Figure 7. Photograph of 5 micron thick ESR ribbon, taken by back illumination.

Figure 8. 5.6cm and 10.0 cm wide silicon ribbons grown by ESR.

stable and reproducible requiring little or no operator intervention during growth and a minimum of effort during startup. In fact, the startup consists primarily of turning the speed dial up from zero to full speed over apporximately 30 seconds time. In most recent furnace designs, radiation shields block the view of the ribbon until it is 4-5cm above the growth interface, and only an edge view is available. Thus, a minimum of visual cues are needed or used during the growth.

As anticipated, the temperature control requirements have been found to be quite liberal, with ribbon successfully grown over a temperature range of $\pm$ 10°C.

The control of ribbon width is inherent to the ESR process and width tolerances are of the order of $\pm$ 0.010 cm. Ribbon thickness across the width is well controlled as illustrated in Figure 9 which shows a thickness profile across a 5.6 wide ribbon of 120 microns average thickness. The thickness nonuniformities are due to melt temperature inhomogenities across the ribbon width which are of the order of $\pm$ 3-5°C. This degree of thickness control is quite adequate, however, further refinements in thickness control are expected.

3.4 Thermally Induced Stresses and Ribbon Buckling

Thermally induced stresses are a major concern in ESR ribbon growth and as such are discussed in Chapter 5 which is devoted to the problem. In brief, the problem is manifested in three ways: buckling of the ribbon (non-flatness), residual stresses which compromise the handling characteristics of the ribbon, and reduced electronic performance due to high dislocation density.

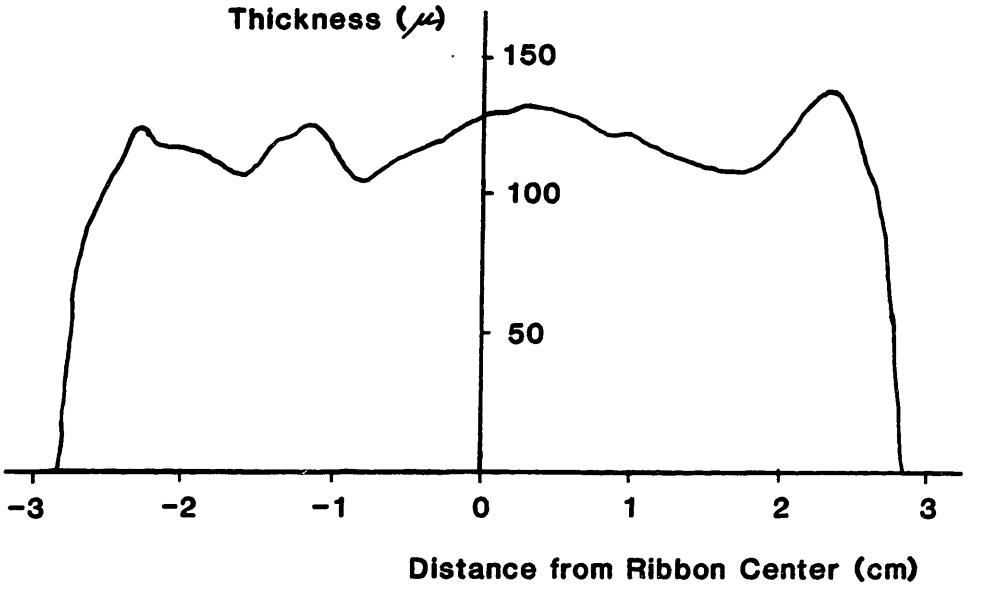

Figure 9. Thickness profile across 5.6 cm wide ESR ribbon. Detector is approximately 3 mm diameter.

The severity of the buckling problem increases with increasing ribbon width and decreasing ribbon thickness. In 2.5 cm wide ribbon, buckling is never observed until ribbon as thin as 50 microns is grown. In 5.6 cm wide ribbon, the ribbon is substantially flat for 200 micron thicknesses and above, but can demonstrate significant buckling when grown 100 microns thick. The experience base with 10.0 cm wide ribbon is more limited, however, it is clear that 100 - 125 micron thick 10.0 cm wide ribbon is extremely buckled, with buckling wavelengths of typically 7-10 cm and amplitudes (peak to trough) of 0.6 cm.

3.5 Grain Size and String Material

In general, the structure of ESR ribbon is determined by nucleation at the strings and propagation of this structure toward the center of the ribbon, resulting in large grains at the ribbon center and small grains near the ribbon edges. The concave downward shape of the growth interface forces the nucleated structure to propagate toward the center of the ribbon as grain boundaries tend to grow orthagonol to the growth interface. As the interface curvature is determined by capillary effects, (see Chapter 7) its shape and the nature of the propagation of nucleated structure are difficult to alter.

As the ribbon width increases, there is a larger center flat zone in the interface shape. This flat zone combined with more space between the strings for grains to coalesce and grow leads to larger grain sizes in wider ribbons. Typically, center grain sizes in 2.5 cm wide ribbon are 2-3 mm wide and 2-3 cm long, while 10.0 cm wide ribbon shown grains up to 2 cm wide and 3-5 cm long.

It is important to note, however, that even in the region immediate to the string where grain size is the smallest, it is sufficiently large so that grain size is not the principal factor controlling photovoltaic efficiency. The nature of the grain structure may be best understood by reference to Figure 20 in Chapter 6.

Cross-sectioning of ribbon samples has shown that the grain boundaries run through the thickness from one face to the other. This type of structure is vital to good electronic performance as grain boundaries lying within the thickness act as trapping sites for photogenerated carriers.

An important factor in determining the nature of the grain structure of ESR is the selection of string material, and the factors influence this selection are discussed in greater detail in the following chapter.

CHAPTER 4

ESR GROWTH - APPARATUS AND MATERIALS

4.1 Introduction

The growth of ESR silicon ribbon requires the design and construction of a specialized furnace, with particular attention to the selection of the materials of construction used. Also of vital concern is the selection of the string material.

These issues, are discussed below, as well as a summary of operating experience with the equipment.

4.2 Furnace Construction - Material Requirements

The primary criteria governing the selection of materials of construction for ESR silicon growth are as follows:

1. The materials must tolerate high temperatures as silicon melts at 1420°C.
2. The materials must not contaminate the melt and the ribbon.
3. The materials must be reasonably priced and machinable, or amenable to others means of fabrication.

The high temperature requirements limit the choice to the refractory metals such as molybdenum, tungsten, tantalum, graphite and other forms of carbon and a variety of ceramic materials including silicon carbide, silicon nitride, silicon dioxide (quartz), boron nitride, and boron carbide.

The requirement of non-contamination of the melt dictates critical design constraints as extremely low concentrations of metallic impurities can destroy the electronic properties of solar cells. For example, if molybdenum is present in silicon in concentrations of 0.1 parts per billion or more, the photovoltaic performance of the material will be severely compromised.[18] Such trace quantities may even be transported by oxidation of the metal surface and subsequent transport of the oxide. Primarily, for this reason, the use of refractory metals has been avoided in ESR furnace design and graphite has been chosen as the primary material of construction.

Due to the high reactivity of molten silicon, only two materials are suitable for use as crucibles; graphite and quartz. Graphite is expected to react slowly with silicon and form a dense layer of silicon carbide at the reaction interface while releasing carbon into the bulk of the melt. Carbon is not particularly detrimental to the electronic properties of silicon, as both have four outer shell electrons. Quartz crucibles are also slowly dissolved in molten silicon and release oxygen into the melt. The microelectronic industry has used quartz crucibles exclusively and, hence, the established route would be to do the same. Nonetheless, graphite was chosen as the crucible material primarily because it will permit the fabrication of crucibles with specialized and detailed features, while quartz may only be easily fabricated in the form of simple liners, etc. Additionally, a quartz crucible can last only about one day, while a graphite crucible can be expected to be used for at least ten days.

4.3 Furnace Design Criteria and Philosophy

One requirement unique to ESR growth is the introduction of strings to the growth area. While, the strings might be introduced through the melt surface, around a pulley submerged in the melt and back up through the melt surface, threading the string around the pulleys from outside the furnace would be difficult. Further, the string materials available for use with silicon are not amenable bending in tight radii. Thus, it was considered imperative to devise a method of string introduction which would allow the string to travel a straight line through the system. Further, a method was needed of readily introducing the strings from outside the furnace so that growth might be quickly restarted if stopped for any reason.

The solution developed was to provide for a hole in the crucible bottom for each string to pass through and to retain the melt in the crucible by capillary action. This approach is especially effective for silicon as it has a very high surface tension to density ratio (over a factor of 4 greater than that of water), and, graphite is well wetted by silicon. Nonetheless, capillary sealing of the crucible bottom does dictate that the melt depth be kept fairly low. In practice, a melt depth of approximately 1 cm is maintained which provides for a safety factor of approximately three.

Crystal growth furnaces are typically heated by one of two methods, either radio frequency induction heating or resistance heating as it allows for the construction of highly specialized geometries and the careful direction of heat application, while induction heating is

usually limited to a cylindrical geometry. The use of resistance heating thus allows for the design of a rectangular system in keeping with the rectangular geometry of ribbon. The rectangular format adopted for ESR furnace design contrasts sharply with the cylindrical design associated with Czochralski growth equipment and this difference is one of the key factors influencing system design.

A further criterion was to minimize furnace power consumption so as to achieve system simplicity and operating economy. The most common approach to resistance heating is to surround the crucible with a large graphite heating element, usually in a cylindrical geometry. However, this must of necessity lead to the use of more power than the minimum required to keep just the crucible and must be run at a higher temperature than the crucible if it is to communicate heat to it. Therefore, the furnace was designed to provide for heating the crucible via heater rods, which are passed through holes in the crucible body. In this manner, all the heat dissipated by the heater is intercepted by the crucible and the size of the heated material is kept to a minimum.

The final design criterion, the most difficult to specify, is that the design be scalable to larger sizes and adaptable to improvements of the technology such as the addition of melt replenishment capability. In a sense, these requirements provided a strong impetus toward a simple design with a minimum of parts (always a good idea anyway) so that future additions would not create an impossibly complex system.

4.4 Furnace Construction and Implementation

An ESR furnace consists basically of a support base, the hot zone consisting of crucible, heating and insulating elements, a protective shell, a crystal puller, a power supply, and all associated electronics.

Figure 10 presents a photograph of the new furnace designed and constructed for ESR growth of up to 10 cm wide silicon ribbon. Figures 11 and 12 shows sequential assembly photographs of the hot zone from the 2.5 cm ESR furnace. The design of the hot zone in the 10 cm furnace is similar in concept.

The largest component of an ESR growth furnace, and one of the least critical, is the outer shell itself. The shell serves prinicpally to contain the argon atmosphere necessary to prevent oxidation of the hot components. The shell must be water cooled as it must absorb the bulk of the power dissipated by the hot zone. Typically, it is made of stainless steel.

Mounted to the base of the shell is a graphite pedestal, which serves to support the hot zone components and to thermally isolate them from the water cooled shell. The pedestal provides the support and location for the majority of the hot zone components including the crucible.

The focus of the furnace design is the crucible itself. This one piece performs the multiple functions of containing the melt, providing for string introduction through the crucible bottom, receiving and

Figure 10. Photograph of ESR furnace used to grow 5.6 cm and 10.0 cm wide ribbon.

distributing the heat radiated by the heating rods which pass through it, and providing for the accurate relative location of vital components.

The crucible is supported by legs which slip fit into the pedestal. The center of the crucible is fixed by a tube which passes up through the center of the pedestal and screws into the bottom of the crucible. This tube extends through the pedestal and doubles as a housing for the temperature sensor which measures the temperature of a cavity in the crucible immediately under the growth area. Thus, a thermocouple or radiometric temperature sensor may be inserted into the tube from outside the furnace with guaranteed alignment and easy servicability. Two of the legs restrain the crucible from rotation, thereby completing its location.

The pedestal also supports the insulation pack which surrounds the crucible on the bottom and the sides. This pack is made of a fibrous graphite material with a void fraction of approximately 90%. The top of the crucible is insulated by graphite radiation shields so as to prevent melt contamination from particles which might fall from the fibrous material.

The pedestal provides the support for the contact blocks which distribute current to the heater rods which pass through the insulation pack and through the holes in the crucible body. The contact blocks are mounted to the pedestal with electrically insulating bushings so as not to short out through the pedestal.

The electrical power to the heaters is provided by a rugged and somewhat oversized 20 kilowatt D.C. power supply purchased from a manufacturer of equipment for the plating industry. A D.C. supply was chosen as it allows for the use of three phase A.C. to power a single phase (two terminal) load. Additionally, it was previously determined that when powered by a single phase A.C. supply, the thermal response of the heater rods was sufficiently rapid to allow for expansion and contraction of the heaters which caused mechanical vibrations in the melt. The D.C. supply has eliminated these problems.

The strings are held on spools which are mounted on tensioning motors held outside and beneath the furnace shell. The strings are passed up through holes in the bottom of the furnace shell and are guided up to the crucible by guide tubes which pass through the pedestal.

The ribbon itself exits through a simple slit in the top plate and may be pulled either by a stroke puller (for short lengths) or by a continuous roller puller.

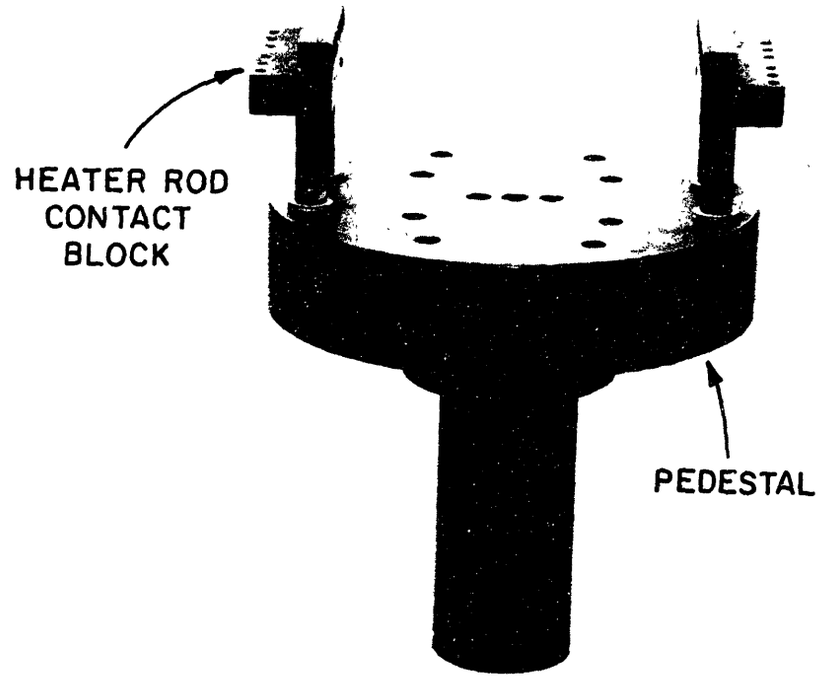

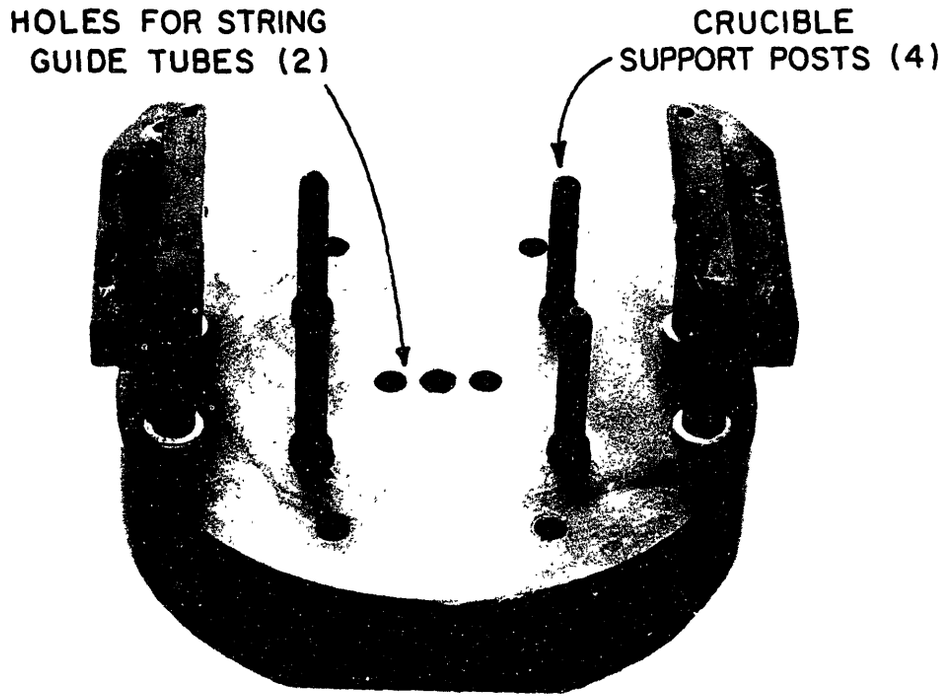

Figure 11. Sequential assembly photographs of hot zone for 2.5 cm ESR growth.

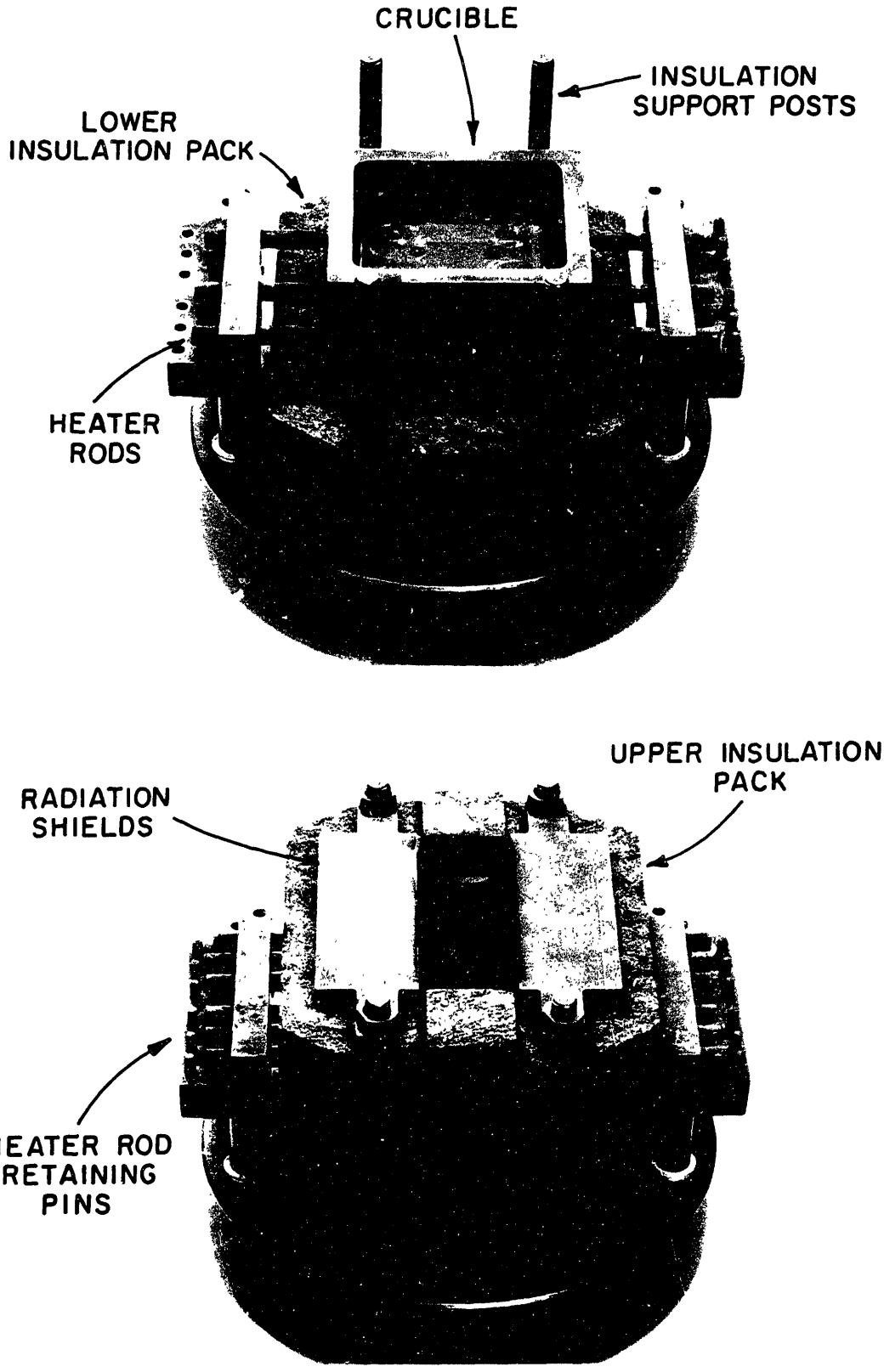

Figure 12. Sequential assembly photographs of hot zone for 2.5 cm ESR growth.

4.5 Operating Experience

The operation of the two ESR growth furnaces has been very satisfactory in all regards. In over 400 hours of operating experience with the 2.5 cm furnace the insulation pack was changed once because of a design change. All other hot zone parts except the crucible were used throughout the over 30 runs conducted in the furnace. The parts show little degredation, except the heaters, which have begun to show oxidation induced pitting. More attention to argon quality and enclosure should extend heater life considerably.

The grade of graphite used for the crucible has a considerable mismatch of thermal expansion with respect to silicon and therefore fractures upon cool down if any silicon remains in it after the growth run. However, by growing all the material out it was possible to save most crucibles, etch the remaining silicon out and remove the remaining silicon cardibe layer during a halogen purification process (performed by a vendor). In this manner, crucibles have been reused three times. The dissolution rate of graphite in silicon is such that runs of several weeks duration should be feasible in the future.

The temperature control in the new 10.0 cm furnace is approximately $\pm$ 1^{o}C at the point of measurement; more than sufficient for ESR growth. Temperature profiles of the hot zone have been taken by passing a small thermocouple through holes drilled along the length of a dummy crucible. This technique has been used to guide a tailoring of the heater rods to provide for a total temperature span over the entire crucible of

approximately $\pm 10^{\circ}C$ and a span within the growth region of approximately $\pm 3^{\circ}C$. The heater rods are tailored by varying the resistance along the length of individual rods and varying the total resistance of each rod with respect to the others. Temperature profiles in a crucible containing silicon are likely to be more uniform than those obtained by profiling a "dummy" crucible as convection currents in the silicon should homogenize melt temperatures.

The power consumption of the 10.0 cm furnace is approximately 5 kilowatts during growth, a low level for a furnace operating at $1400^{\circ}C$. At such power levels, the cost of electricity becomes a negligible quantity in the cost of wafer produced.

A larger cost component is that associated with argon utilization. In current design a simple slit is provided at the top of the furnace through which the ribbon and argon exit. This slit must be substantially closed during ribbon growth, but must occasionally be opened between ribbon lengths, thereby admitting air and oxygen to the system requiring a high argon flow. It is expected that in totally continuous operation, this problem will be somewhat lessened in magnitude.

In summary, the furnace operation has been extremely reliable and consistent. After a short time, the operator develops a clear sense of confidence in the equipment.

4.6 String Material Selection

In order to serve as a string material for ESR growth a material must meet the following criteria:

1. It must be available and economical
2. It must tolerate the necessary temperatures (1400^{o}C for silicon)
3. It must be chemically stable in silicon
4. It must be at least paratially wetted by silicon
5. It must not contaminate the melt
6. It must have a reasonable match of thermal expansion coefficient to silicon

A list of materials eligible under criteria 1-4 includes, graphite, carbon, vitreous carbon, silicon carbide, silicon nitride, silicon dioxide (quartz), boron, and silicon carbide coated boron. While this list is not excessively long, each material may be fabricated in many forms, e.g., multifilament or monofilament, and by many technologies, e.g., spinning, extrusion or chemical vapor deposition. Further, properties may be tailored as per grain size, fiber diameter, etc. Thus, the possibilities are numerous.

In fact, ESR has been successfully performed using all the above mentioned materials. In most cases, many forms of each material were tried, and a total of approximately 15 materials have been used for ESR growth.

The range of wettability of these materials spans the range from grahite, which is extremely well wetted by silicon, to quartz, which is only partially wetted and in fact results in ribbon where the silicon is only attached to the inside of the string, the outer surfaces remaining clear and transparent.

Melt contamination has not been observed with any of the materials, although in several cases, the lengths used have been too short to be certain that contamination was not taking place.

The issue of thermal expansion match to silicon is of great concern, as excessive mismatch will lend to substantial stress in the ribbon edges and severe handling problems. The expansion coefficients of the tested materials vary over a very wide range including materials both higher and lower in expansion than silicon. Appendix B contains a discussion of the measurement of these expansion coefficients and the resulting data.

Several additional issues concern string material selection. For example, there appears to be a substantial difference among string materials on the nature and amount of nucleation which takes place at the ribbon edges. Thus, quartz string has been found to result in relatively little nucleation while graphite strings produce a great deal of random grain nucleation.

CHAPTER 5

THERMAL STRESS

5.1 Introduction

As noted previously, thermal stress is one of the major problems remaining in ESR growth. These stresses arise primarily from the motion of the ribbon through temperature fields which include regions of high gradients and curvatures (first and second derivatives with respect to displacement). To some measure regions of high gradients are unavoidable as a high temperature gradient is required in the ribbon at the growth interface. In fact, as shown in Chapter 7, the maximum growth speed attainable is proportional to the gradient in the ribbon. For example, a growth speed of 3 cm/min requires a gradient of approximately $900^{o}C/cm$. Clearly, gradients of this magnitude cannot persist for long and high curvatures are the result.

The thermally induced stresses arise primarily from the curvatures in the temperature field while the gradients do not play a direct role.[19,20] This may be understood by reference to Figure 13 below which shows a ribbon cut into three strips and subjected to temperature profiles with $\frac{d^2T}{dz^2} = 0$ and $\frac{d^2T}{dz^2} \neq 0$ respectively. As may be seen, when there is no curvature in the profile, the pieces can fit together with no distortion. However, with curvature, the pieces would have to undergo bending stresses before if they were to become contiguous.

As the ribbon cools from the melting point to room temperature, it passes through the complete range of plastic and elastic behavior available to a solid. The problem is therefore highly complex and can

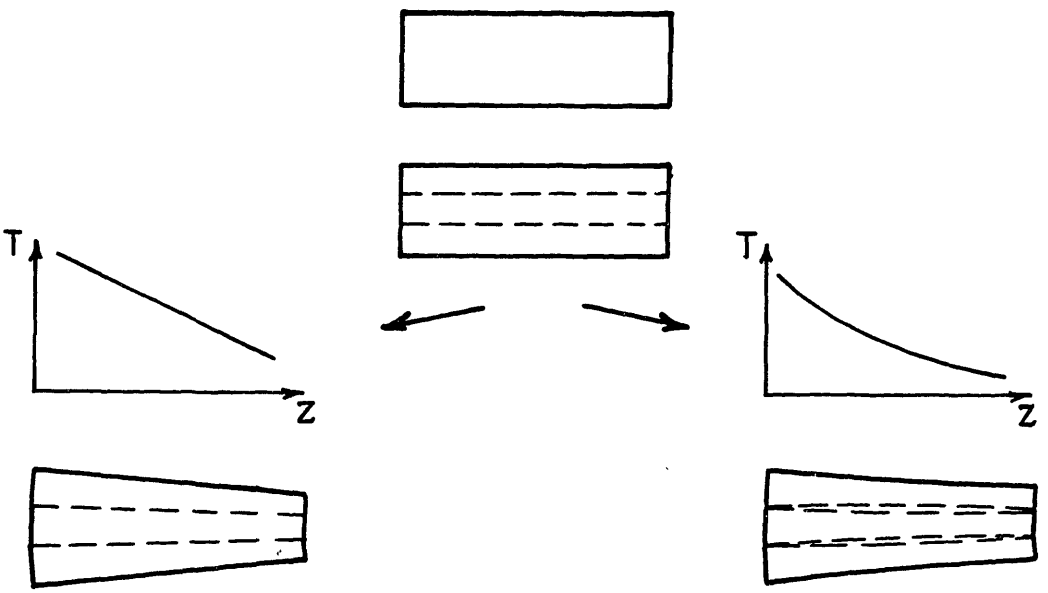

Figure 13. Origin of thermal stress in ribbon growth. A ribbon is cut into three immainary strips, subjected to linear and nonlinear temperature profiles and reassembled. (Assumes that expansion coefficient is not a function of temperature.)

manifest itself in many different ways. Stresses arising within the plastic region can cause the ribbon to buckle out of its plane and result in permanently deformed ribbon. If the stresses occuring in the plastic region are insufficient to cause buckling, they may cause deformation within the plane resulting in increased dislocation densities and reduced electronic performance. In addition, by setting up a zero or low stress state in region of high curvature, plastic flow may result in room temperature ribbon with high residual stresses, by the inverse of the argument presented in Figure 13. Residual stresses caused by this or other mechanisms is undesirable in that ribbon handling properties are compromised.

The problems of thermal stress are common to all ribbon growth methods with only slight differences in the nature of the problem between methods. In ESR, for example, any mismatch of expansion coefficient between string and silicon is a possible additional source of thermal stress. However, it is believed that this effect is so local as to have little influence on the overall problem.

Detailed finite element analyses have been undertaken by others in the ribbon growth field.[21] However, in an effort to keep the problem tractable, many simplifying assumptions have been made concerning the behavior of the silicon as it passes through the full temperature regime. As such, the results can serve only as guidance; they do not define the "ideal temperature profile".

The approach taken in this work to date has been a limited empirical investigation guided by the literature in the field.

5.2 Reducing Thermal Stress

Fundamentally, three approaches are available to reduce the impact of thermal stress:

1. Reduce the gradient at the interface and therefore all gradients and curvature. This has the deterious side effect of reducing growth speeds.
2. Change the shape of the temperature field by reducing and relocating curvature, with attention to the interaction of curvature with temperature controlled material parameters. Change in temperature profiles both along the ribbon length and across the ribbon width will affect thermal stresses.
3. Provide sufficient residence time at high temperatures so as to accomplish annealing of residual stresses.

The experimental work has concentrated on reshaping the critical area of the temperature profile immediate to the growth region by the use of passive radiation shielding which basically redirects the radiation from the melt surface back to the growing ribbon. These shields have been used to effect changes in both vertical and horizontal profiles, with some relatively small reduction in growth speed. Significant improvements in the flatness and handling characteristics were immediately observed in the growth of 2.5cm wide ESR ribbon. Figure 14 shows a multiple exposure photograph of a 90 micron thick ESR ribbon grown with the passive shielding which demonstrates a high degree of flexibility. Improvements were also observed in how readily the material could be scribed into solar cell blanks, a simple but important characterization of material handling properties.

Figure 14. Multiple exposure photograph of flexible 2.5 cm wide ESR ribbon. The ribbon is approximately 90 microns thick.

As noted in Chapter 3, the severity of thermal stress problems increases with increasing ribbon width, and much effort remains especially concerning the buckling of wide thin ribbons. Figure 15 shows four 10cm wide ribbons approximately 125 microns thick grown with different thermal geometries imposed by different radiation shielding geometries. It is clear that buckling is a very severe problem, but that it is highly responsive to changes in temperatue profiles.

A further complication exists in that some of the deviations from flatness in the ribbon may actually be grown in. While the edge positions of the ribbon are fixed by the string positions, the central region is free to wander over the melt surface resulting in the growth of trough shaped ribbon. Thus, if a buckle is initiated by thermal stresses, it may distort the growth meniscus and cause the growth of an exaggerated "buckle". This process is often observed during growth.

5.3 Thermal Stress and Dislocations

As noted previously, dislocations induced by thermal stresses are a major factor limiting the photovoltaic performance of ESR ribbon. As discussed in the following chapter, ESR solar cells are limited primarily by their short circuit current performance. The current performance is limited because of poor diffusion lengths in the material due to large numbers of dislocations which act as trapping centers for the photo generated charge carriers.

Figure 15. Photograph of four 10.0 cm wide ESR ribbons grown with different thermal environments as modified by radiation shielding. The buckling changes with different temperature profiles, but in all cases is severe. Ribbons are approximately 110 microns thick.

CHAPTER 6

SOLAR CELL FABRICATION, TESTING AND RESULTS

6.1 Introduction

The goal of this work is to produce high efficiency solar cells on potentially low cost ESR ribbon silicon. This chapter discusses the fabrication, test results and characterization of ESR solar cells.

As noted below, the conversion of ESR material is as high as 14.0% on 3.5 cm^2 active areas. Novel infra-red laser scanner studies have shown that the performance limiting factor is a high dislocation density in the ribbon material.

6.2 Fabrication Sequence

Solar cells of $1cm^2$ and $4cm^2$ area have been fabricated on ESR ribbon and on single crystal control wafers using a process sequence composed of standard, established techniques. Removal of the string from the ribbon edges is the current practice, but may or may not be required, depending on the nature of the string method and the details of the junction geometry.

First, the wafers are cleaned using a series of standard semiconductor industry cleaning solutions. No etching or surface preparation of any kind is required for the ribbon. Next, the junction is formed by diffusing an n-type phosphorous layer into the p-type wafers. The diffusion is performed in a quartz tube diffusion furnace

using $POCl_3$ as the phosphorous source. A 900°C, 30 minute diffusion results in a junction depth of .5 microns, which is shallow enough to minimize optical absorption in the top layer, but deep enough to provide good sheet conductance in the top layer. As the diffusion results in a junction on both sides of the wafer, the front side is waxed and the back junction is etched off.

Finally, the cells are metallized by electron beam evaporation of titanium and silver to form the front contact. The titanium forms the ohmic contact to the silicon, while the silver provides the necessary conductance. The front contact fingers are formed by evaporation through a shadow mask. The back contact is formed by electron beam evaporation of aluminum. The structure is then sintered at 450°C to enhance the contact quality between metal and silicon. To this point, no cells have had anti-reflection coatings applied to them. The resulting cell structure is shown schematically in Figure 16.

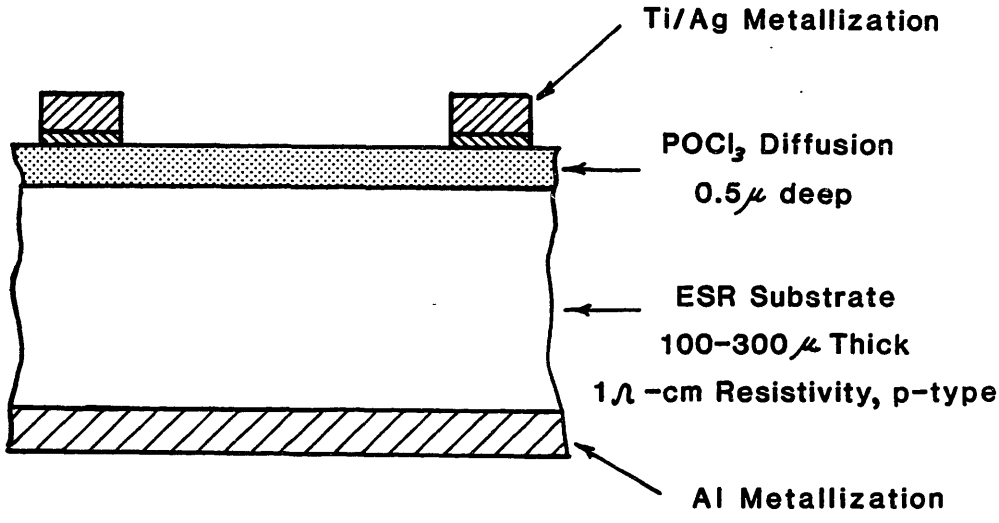

Figure 16. Schematic of construction of ESR solar cells.

6.3 Results

The fabricated solar cells are tested on a solar simulator which uses a tungsten halogen (ELH) lamp to approximate the solar spectrum*. The cells are tested at air mass 1, or AM1 conditions of 100 mW/cm^2 of total solar flux, which approximates peak sunlight conditions. The performance data is taken in the form of a current vs. voltage curve (I-V curve), from which the open circuit voltage (V_{oc}), short circuit current (I_{sc}), and fill factor are measured. Knowledge of the cell area allow for the computation of the short circuit current density and cell efficiency. For a more complete discussion of the inter-relation of I-V curves see Appendix F.

An I-V curve representative of the best performance observed to date on 4 cm^2 ESR solar cells is presented in Figure 17, together with the measured and calculated cell parameters.

Over 50 solar cells have been fabricated on ESR ribbon. Twelve of these are of 4 cm^2 area and the remainder are of 1 cm^2 area. These cells have been fabricated on both 2.5 and 5.6 cm wide ribbon from six different growth runs ranging over a wide variety of condition, including the very first growth run performed with silicon. Three of the runs were performed "clean", that is, with purified graphite furnace components and special attention to cleanliness. No difference in performance was observed between 1 cm^2 and 4 cm^2 cells fabricated on material from the same growth run.

---

*ELH lamps are slightly richer in the red than sunlight, but are a convenient and accepted test standard.

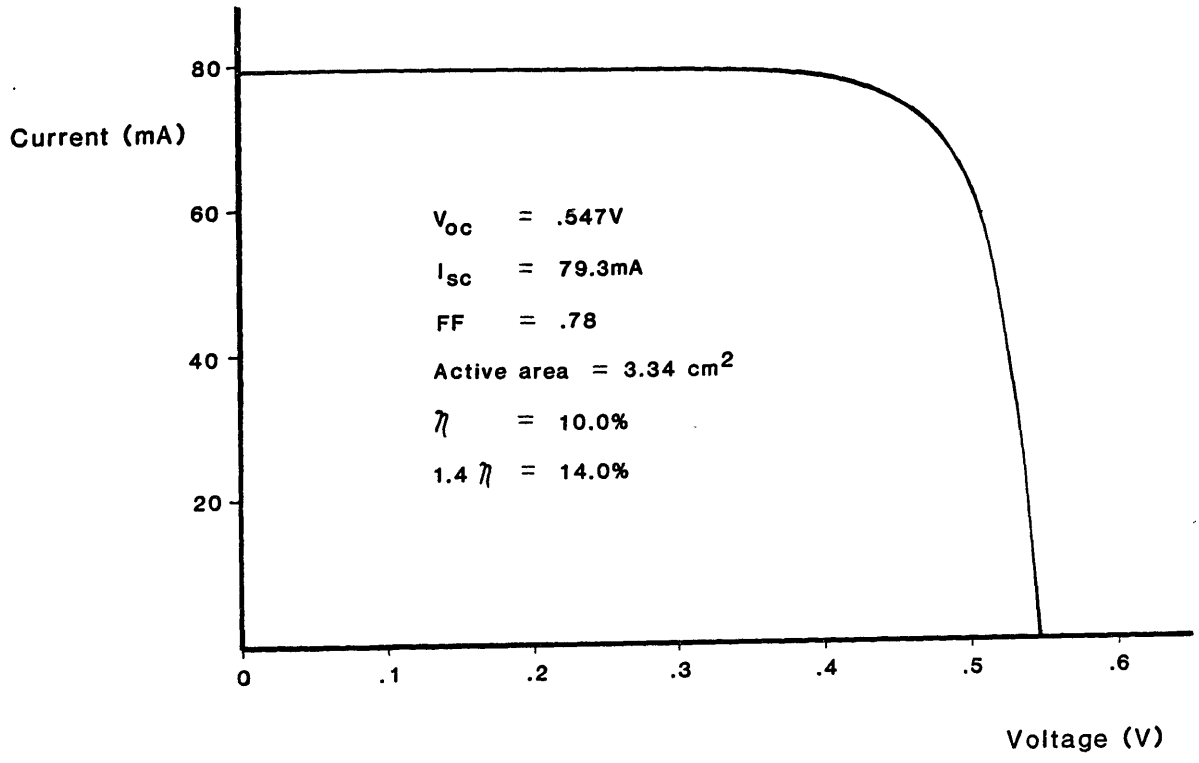

Figure 17. Current-voltage (I-V) curve of best ESR solar cell.

The ESR solar cells have been divided into four groups. Group A consists of six cells made on material from "dirty" runs performed before stress reduction efforts were undertaken. Group B consists of 24 cells made on material from "clean" runs before stress reduction efforts. Group C consists of 21 cells made on material from "clean" runs performed with stress reduction apparatus in place. Group D consists of a small sample of cells made very recently on material with reduced dislocation densities. The results are too new and too few to present as statistically meaningful, and they are therefore excluded from the Table below. However, they are extremely promising, as the worst cell of Group D is comparable in performance to the best cell previously made. The I-V curve of Figure 17 is from this group of cells, and is representative of the best performance achieved to date on a 4 cm^2 ESR solar cell.

The results are presented in Table 1 below as averages ± 1 standard deviation. Also presented are typical values for co-processed single crystal control cells. The short circuit current densities and efficiencies are based on active device area, and have been corrected for the absence of an anti-reflection coating (that is, they have been multipled by 1.4, the standard gain achieved by the proper 1/4 wavelength coating applied to the cell). An occasional cell is found to have poor performance, and these cells have in all cases been found to have cracks in the substrate which result in shorted p-n junctions. In cases which permited, these cells have been repaired by etching around the crack, and the performance has come up to typical levels. Cells in which the crack location did not permit for repair have not been included in the data.

Table 1 Active Area Cell Efficiencies for ESR and Control Wafers

(Corrected for AR Coating)

	Group A 6 cells "high stress" "dirty"	Group B 18 cells "high stress" "clean"	Group C 21 cells "low stress" "clean"	Single Crystal Control
V_{oc} (volts)	.516 ± .019	.526 ± .011	.525 ± .010	.585
J_{sc} (ma/cm^2)	23.7 ± 1.5	24.8 ± 1.9	25.9 ± 1.5	35.7
FF	.73 ± .01	.74 ± .03	.76 ± .02	.78
η (%)	8.9 ± 1.0	9.7 ± .9	10.3 ± .7	16.3

First, note that the "dirty" material is somewhat lower in performance that the "clean" material, as expected. However, even this material displays reasonable performance. Similarly, the low stress (and therefore presumable low dislocation density) material is better in performance than the high stress material, but the difference is not as great as hoped for based on the very substantial improvement observed in mechanical handling properties (see Figure 14, Chapter 5).

Nonetheless, the difference is significant and occurs primarily as an improvement in short circuit current density as expected for improved diffusion lengths. The improvement may also be seen in Figure 18 which presents histograms of the cell efficiencies for Groups B and C. These histograms also serve to illustrate the tight performance range of ESR cells, especially those of Group C. As noted, the preliminary results of Group D indicate that further reduction in dislocation density has resulted in further performance improvement.

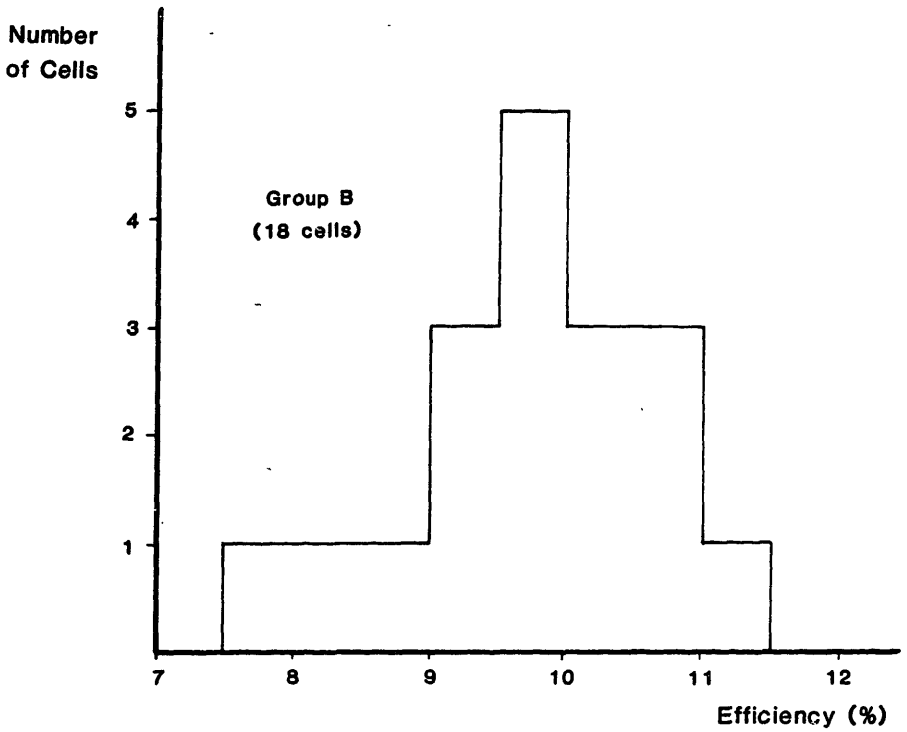

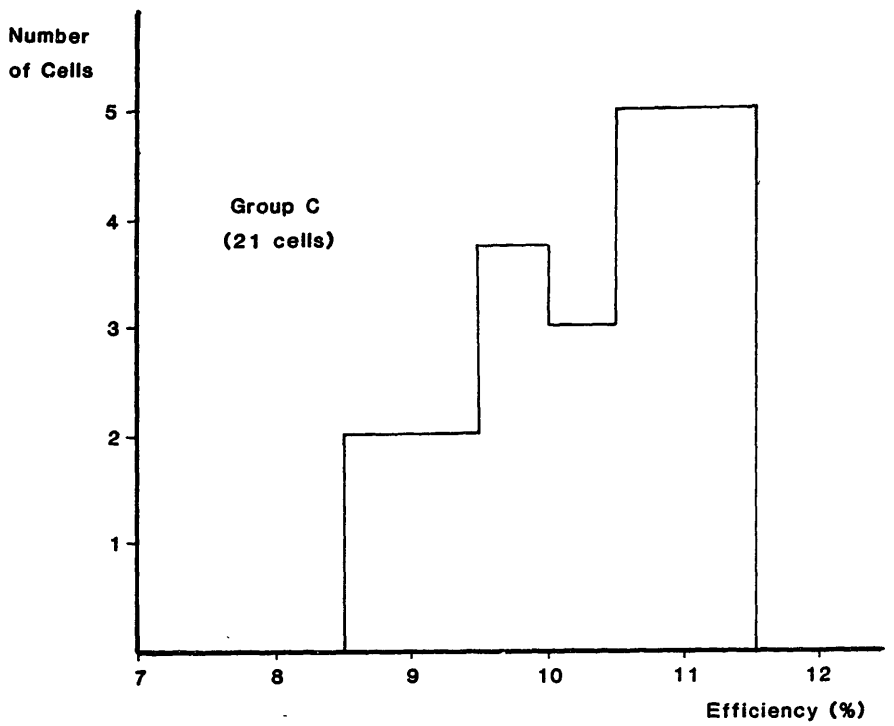

Figure 18. Histograms of cell efficiencies for ESR solar cells. Group B is "high stress", "clean". Group C is "low stress", "dirty". Efficiencies are based on active area and are corrected for AR coating.

As the above data indicate, consistency of cell performance on ESR material has been very good. Each step taken to improve performance such as improved cleanliness or reduced stress and disloation density, has resulted in real efficiency gains. Consistent performance is also observed from beginning to end of a growth run.

While the performance of ESR cells to date is good, there is room for improvement as compared with single crystal material. Examination of Table 1 shows that the performance of ESR cells is primarily limited by short circuit current response, and the next section discusses diagnostic efforts designed to examine this poor current response.

6.4 Diagnostics and Characterization

When a solar cell demonstrates performance limited by poor short circuit current characteristics, the problem is likely to be poor diffusion lengths in the starting material (see Chapter 1). As such, considerable effort was invested in developing methods of measuring diffusion lengths on a local basis so as to facilitate correlation between electronic performance and structural features of the ribbon.

An infrared laser scanner was constructed which provides a detailed photographic map of the electronic performance of the material under test. The photograph is actually a gray scale representation of the short circuit current generation of the material in response to infrared light with a spatial resolution of aproximately 25 microns (for details see Appendix E). The short circuit current response to infrared light is monotonically but nonlinearly related to the diffusion length in the material.[22]

Figure 19 shows such scans of $1cm^2$ ESR solar cells. The white areas are the best in performance and the black the worst. The gray levels span the range from less than five microns diffusion length to greater than 50 microns diffusion length for full white. The top collecting electrode is clearly seen as an area of no photovoltaic response at all as no light can penetrate the metal. As may be seen areas of good and bad performance are often contiguous, and commonly correspond to adjacent grains. Active, or poorly performing grain boundaries are also visible in places, confirming the excellent resolution of the measurement technique.

The most useful and unique application of the laser scanner has been in the evaluation of ribbon in the as-grown condition with no fabricated solid state junction. This is accomplished by employing an electrochemical junction consisting of an electrolyte in contact with the ribbon and a counter electrode.[23] In this manner, the time consuming junction formation step is avoided and the electronic measurements are not confused by the high temperature treatment associated with junction formation.

Figure 20 shows an electrochemical junction laser scan of 2.5 cm wide ESR ribbon. The scan extends to the edges of the ribbon and the small grains caused by nucleation at the string are clearly visible. Also apparent, is the manner in which the structure propogates toward the center of the ribbon as growth proceeds (the photo is oriented as if the

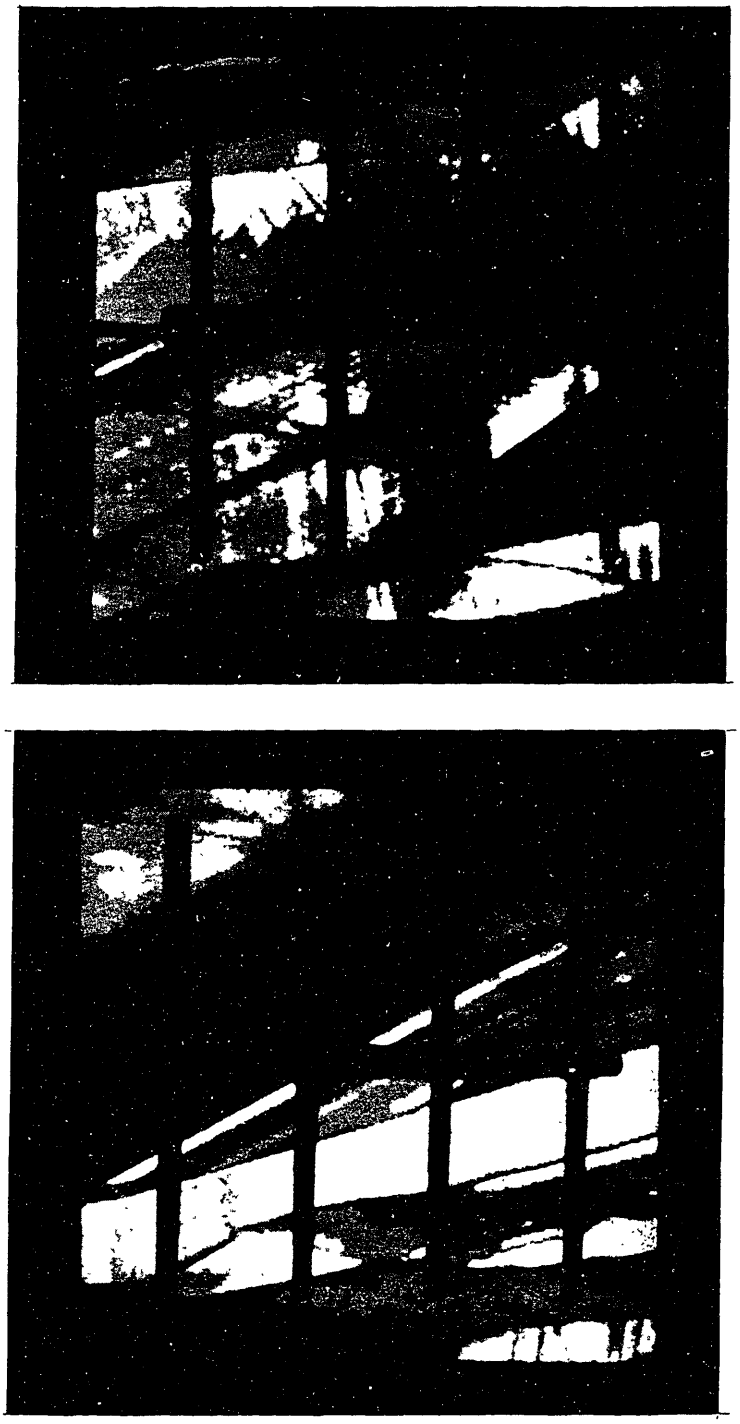

Figure 19. Infra-red laser scanner photographs of 1 cm^2 ESR solar cells. Photographs show the local electronic performance of the ESR material as gray tones; white corresponding to the best performance and black to the worst.

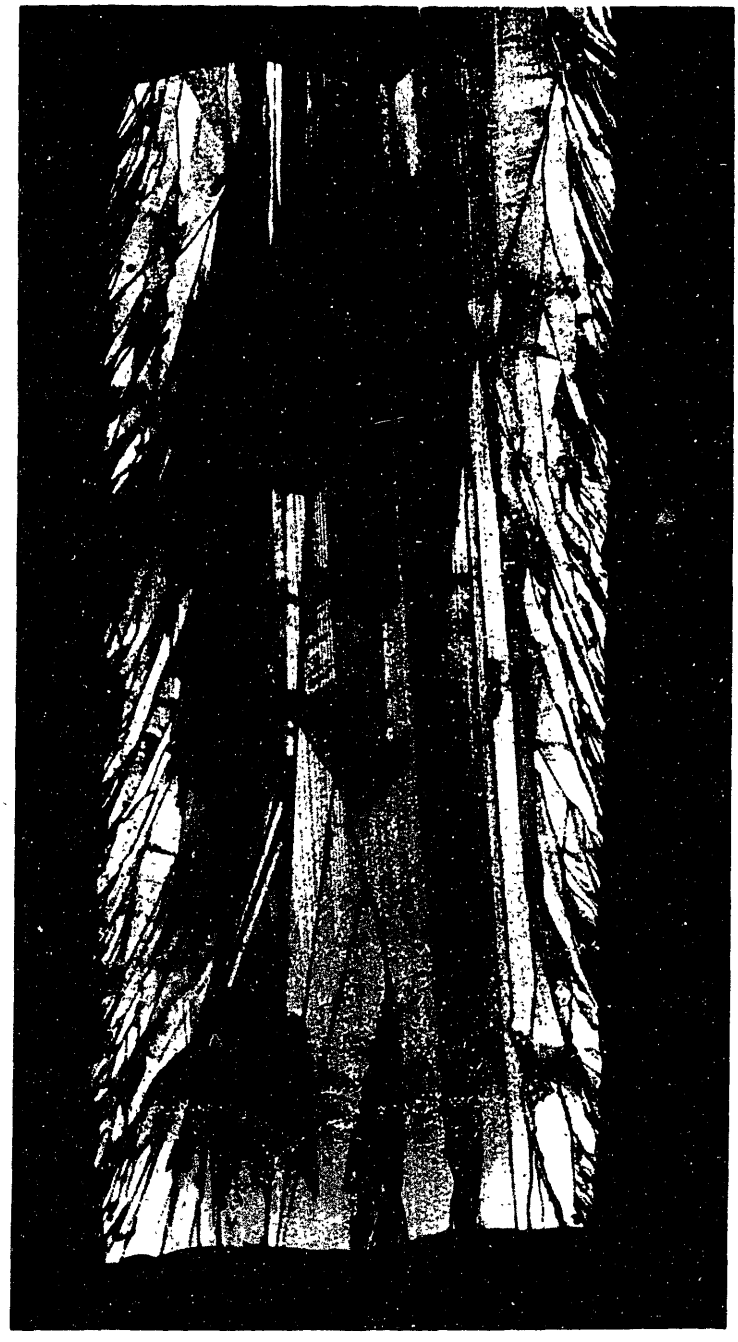

Figure 20. Infra-red laser scan of 2.5 cm wide ribbon, taken by the electrochemical junction technique. Ribbon is oriented as if growing upward.

melt were to the right). As the grains propagate toward the center, they coalesce and grow in size, resulting in the largest grains in the center of the ribbon. It is of importance to note that the overall performance is not greatly different from center to edge of the ribbon. In fact, the performance of the edge regions is limited primarily by active grain boundaries as the intra-grain performance is very good. Thus, solar cells may be fabricated to the very ribbon edge with no loss of performance.

After laser scanning, the sample may be etched in a special formulation designed to reveal dislocations as etch pits. The etch used for this work is the "Wright" etch.[24] The density of dislocations on the etched sample may then be compared with the photoresponse map produced by the laser scanner. Such examinations have demonstrated a one to one correlation between electronic performance (diffusion length) and dislocation density, extending to the minutest of details.

The experiments show that ESR solar cell performance is limited by the dislocation density of the as grown ribbon due to the limiting effect of dislocation density on diffusion length and therefore solar cell current response. As noted previously, this degraded electronic performance is a further detrimental effect of thermal stress as the dislocations are the result of stresses occuring in the ribbon while it is at a temperature high enough to allow for plastic strains to result.

CHAPTER 7

ESR GROWTH-THEORY

7.1 Introduction

Three distinct theoretical aspects of ESR will be discussed in this chapter with details for the first two topics presented as appendices:

1. Steady State meniscus height and shape
2. Steady State thickness as a function of speed
3. Dynamic analysis

Presented below is a list summarizing the notation used throughout the theoretical discussion of ESR growth in this chapter and in the appendices.

7.2 Notation, Definitions, and Material Constants

The numbers in parentheses are the values, where relevant of the material values for silicon. Typical units are given for all other parameters. The geometric parameters are summarized in Figure 21.

ΔP - the pressure difference across the meniscus surface [dyne/cm^2]

R_1, R_2 - the principal radii of curvature of the meniscus surface [cm]

g - acceleration of gravity [cm/sec^2]

s - meniscus height, ie, the maximum height of the liquid of the meniscus [cm]

t - ribbon thickness [cm]

V_p - pulling speed; the rate at which the ribbon is withdrawn from the furnace [cm/sec]

V_g - growth speed; the rate of advance of the solid liquid [cm/sec]

ϕ - meniscus angle; the angle between the meniscus surface and vertical [^{o}]

γ - surface tension of the molten material material (720.dyne/cm)

ρ - density of the liquid (2.53g/cm^3)

L - heat of fusion of the solidifying material (1806.J/g)

ϕ_o - the meniscus angle required for constant thickness growth (11^o)

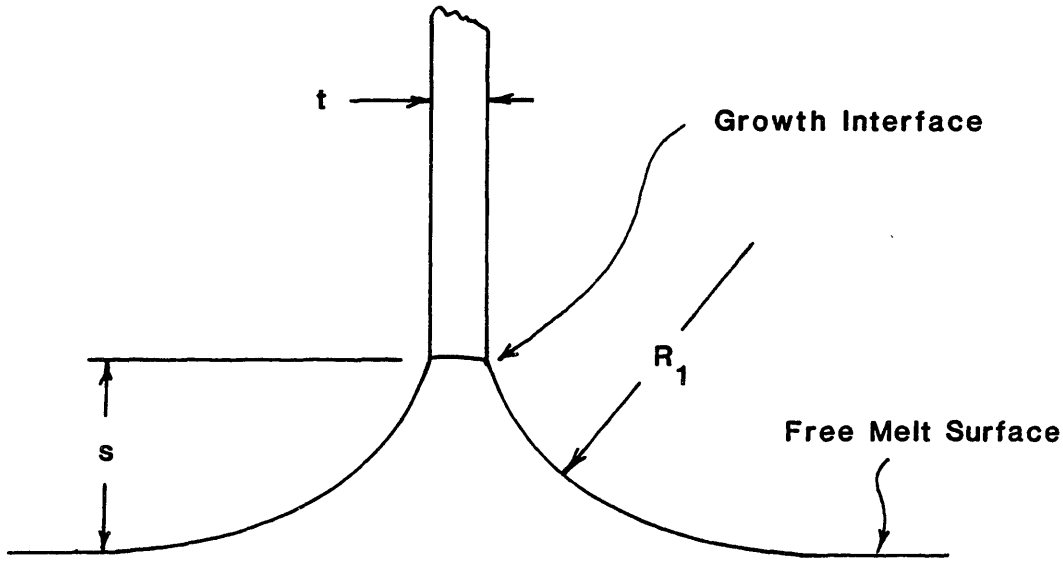

Figure 21. Schematic cross section through the thickness of an ESR ribbon, in the center of an infinitely wide ribbon.

7.3 Steady State Meniscus Height and Shape

The meniscus is the portion of the melt which extends above the free melt surface and which is supported by capillary attachment to the growing crystal. The shape of the meniscus surface is determined by capillarity as embodied by the Laplace equation:

$$\Delta P = \gamma \left(\frac{1}{R_1} + \frac{1}{R_2} \right) \qquad (1)$$

where R_1 and R_2 are the principal radii of curvature.

The pressure drop across the meniscus surface is due to the metallostatic head of the liquid in the meniscus and is therefore proportional to height above the free melt surface, $\Delta P = \rho g z$.

At the center of an infinitely wide ribbon, as in Figure 21 one of the principal radii of curvature (R_2) is infinite and the problem is greatly simplified. At the ribbon edges, R_2 is finite and small, and is approximately equal to the radius of the string. Further, R_2 and R_1 are of opposite sign at the edges. Since the sum $1/R_2 + 1/R_2$ must be the same for center and edges at a given height above the melt, it follows that R_1 must be smaller in magnitude at the edges than at the center. Therefore, the meniscus height at the edges is smaller than in the ribbon center, resulting in a concave downward growth interface. This interface shape may be seen in Figure 6 of Chapter 3.

While the complete solution for the meniscus shape is complex, and not attempted here, it is most instructive to examine the meniscus height and shape of an infinitely wide ribbon, as the results will apply to most of the width of any ribbon of practical interest.

The boundary conditions on the meniscus at the melt surface and at the crystal are needed for the complete specification of the problem. The meniscus must blend into the melt surface with no discontinuity in slope as no physical discontinuity exists. At the top, where the meniscus attaches to the crystal, however, there can be a discontinuity of slope. In fact, Chalmers, et al[10] have shown for any particular material there will be a characteristic angle of attachment of the liquid to the crystal at the triple junction of liquid, solid, and vapor. For silicon, the angle was found to be approximately 11^{o}. From the definition of the meniscus angle as the angle between the meniscus surface and the vertical, it follows that for constant thickness growth; $\phi_o = 11^{o}$

Thus, the problem consists of integrating the Laplace equation between the two boundry conditions. This problem has been solved analytically and the meniscus height is given as (see Appendix C, or Reference 25);

$$s = [2(1-\sin\phi_o)]^{1/2} \left(\frac{\gamma}{\rho g}\right)^{1/2} \qquad (2)$$

Substituting the appropriate material parameters for silicon:

$$s = 0.69 \text{ cm}$$

Thus, the meniscus height for silicon is quite substantial, and the solidifying crystal is isolated from the bulk of the melt.

The complete shape of the meniscus is shown in Figure 22.[25]

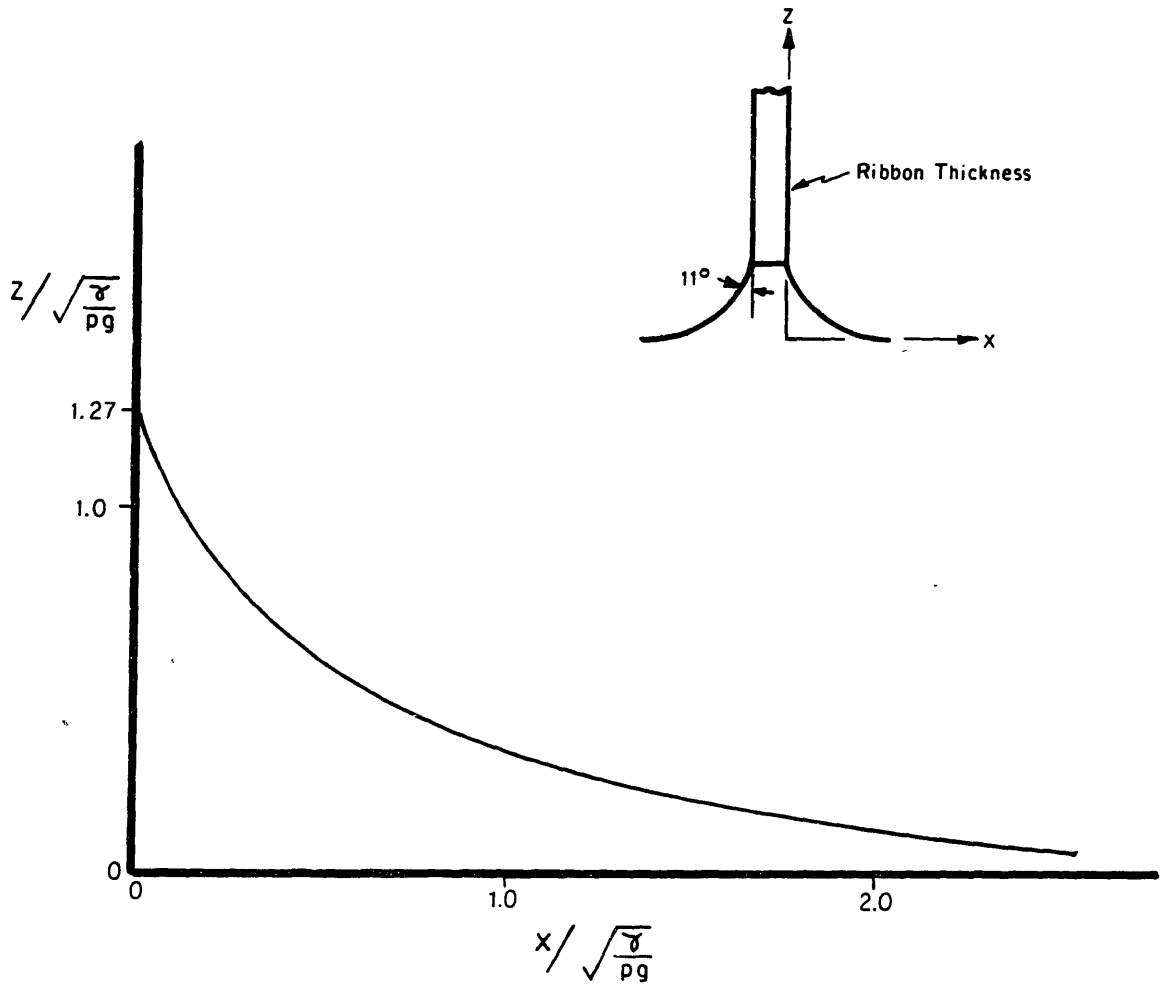

Figure 22. Meniscus shape for growing ESR ribbon.

7.4 Steady State Thickness as a Functon of Speed

The thickness of the growing ribbon is determined by an instantaneous heat balance at the growth interface. Heat is conducted up the meniscus from the melt bulk to the growth interface (Q_{men}), heat is generated at the growth interface by the heat of fusion of the solidifying material (Q_{fusion}) and heat is conducted up the ribbon and radiated from its surface (Q_{rib}). Thus;

$$Q_{men} + Q_{fusion} = Q_{rib} \tag{3}$$

As discussed in Appendix D it is useful and justifiable to ignore the heat conducted up the meniscus in favor of the other two terms as these terms dominate in magnitude and in the strength of their dependence on thickness and speed. The small meniscus contribution results primarily from the thermal isolation afforded by the large meniscus height of ESR growth.

The heat of fusion term is simply proportional to the volume of crystal solidified per unit time. Thus per unit width of ribbon;

$$Q_{fusion} = \rho L V_g t \tag{4}$$

Q_{rib} is determined by the solution of a fin heat loss problem where the ribbon is the fin losing heat by convection and radiation. It may be shown that the heat conducted up a ribbon from the growth interface per unit time and width is given by;[7]

$$Q_{rib} = C_1 t^{1/2} \tag{5}$$

where C is a constant of proportionality.

Combining eqs 4-6 we see that;

$$V_g t^{1/2} = \text{Constant} \tag{6}$$

Figure 23 presents thickness versus speed data for ESR growth run and a $V_g t^{1/2}$ = constant line plotted through the center data point.

From another perspective, the heat conducted up the ribbon is proportional to the temperature gradient in the ribbon at the growth interface and the ribbon thickness. Together with eq. 4 it follows that:

$$V_g = \frac{k}{\rho L} \frac{dT}{dz} \Big|_{\text{ribbon at interface}} \tag{7}$$

This relationship was derived by ignoring Q_{men}, and hence gives the maximum growth speed attainable for a given gradient in the ribbon. It provides estimates useful for thermal stress analysis.

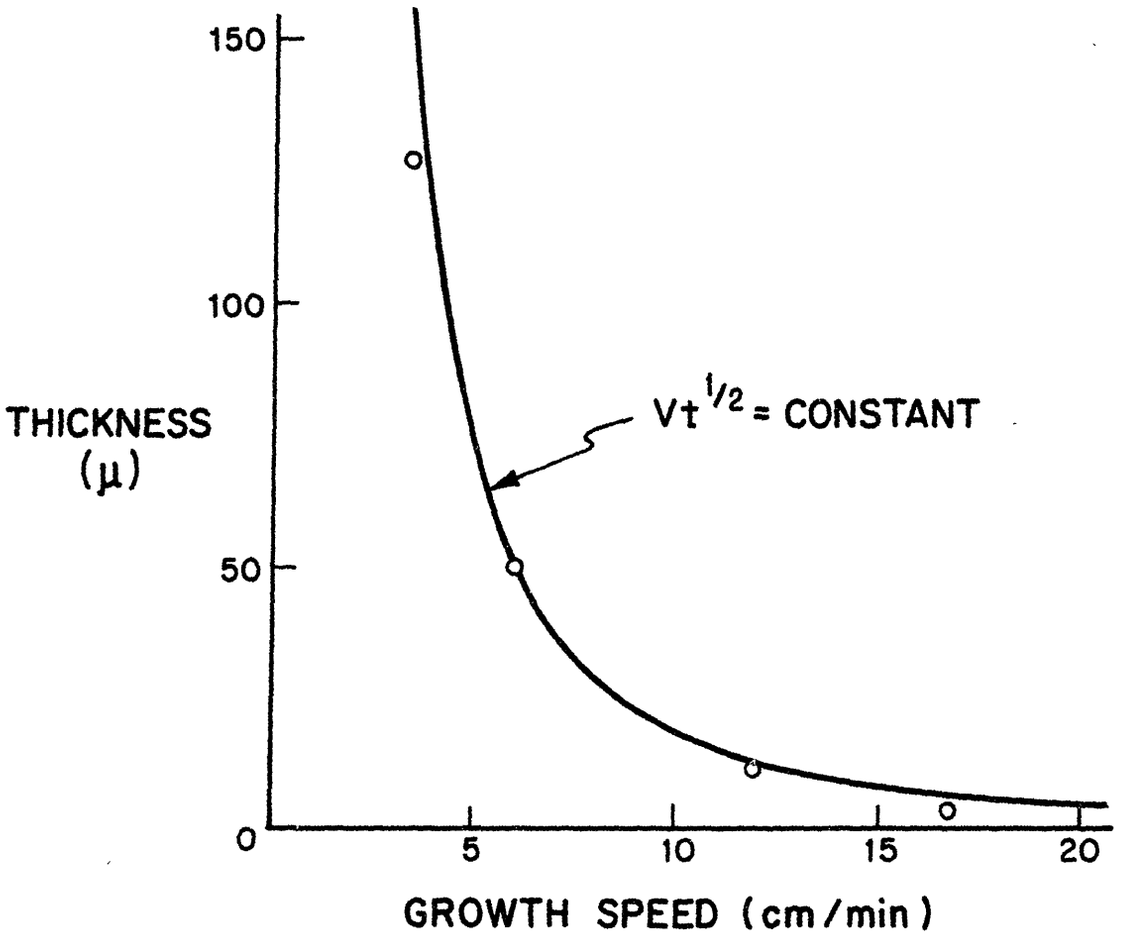

Figure 23. Speed thickness relationship for ESR growth.

7.5 Dynamic Analysis

The intent of this dynamic analysis is to develop a qualitative understanding of the system response to a perturbation from steady state growth, and to examine the absolute stability of the system. The analysis is a process specific application of the generalized dynamic analysis of meniscus controlled crystal growth by Surek.[26]

The variables of concern in a dynamic analysis are indicated in Figure 24a, where subscript "o" indicates steady state values. Figure 24b shows these same parameters with perturbations added to the steady state values eg $t = t_o + \Delta t$. A discussion of dynamic effects divides into two categories; geometrical and thermal/energy balance.

7.5.1 Geometric Considerations

As discussed previously, constant thickness ribbon can only grow with a specific meniscus height, s_o, which is determined by material parameters and is not a function of ribbon thickness. Similarly, a specific value of meniscus angle corresponds to constant thickness growth. This may be understood by noting that the angle between the meniscus surface and the forming ribbon surface must assume a specific material dependent value (for silicon it is 11^oC). Only when the meniscus angle assumes this value ($\phi_o = 11^oC$) will the emerging ribbon have vertical faces and therefore grow at constant thickness.

When the meniscus height changes from its equilibrium value during a transient, the position and shape of the meniscus surface at any given

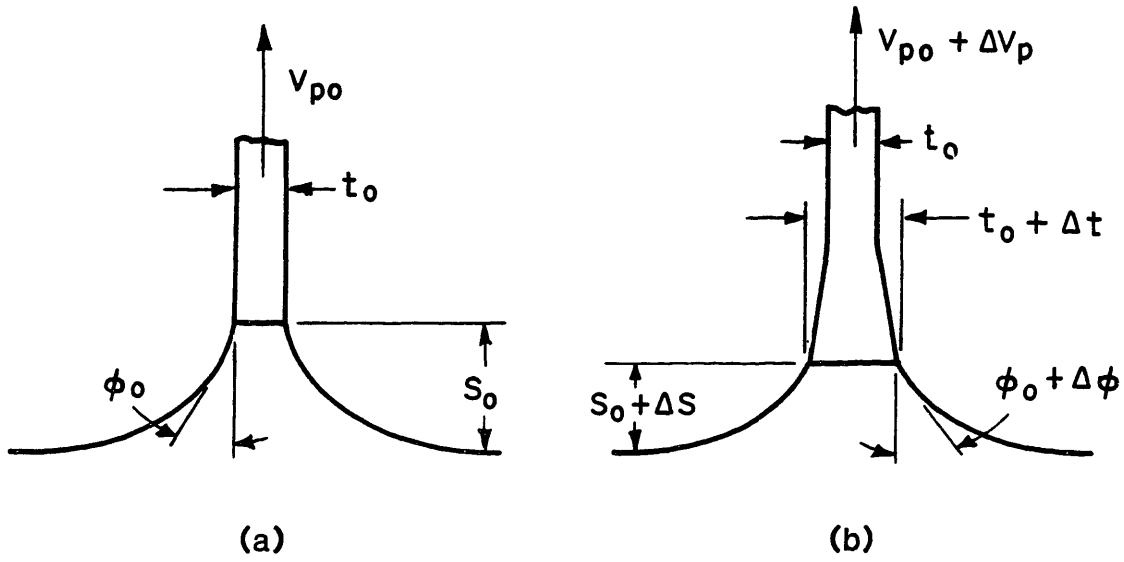

Figure 24. Explanation of the variables used in dynamic analysis.

elevation above the melt is not changed. Rather, the capillarity determined meniscus shape is merely truncated at a different elevation above the melt. Therefore, there exists a specific constitutive relationship between meniscus angle and meniscus height, determined by the shape of the meniscus surface. In linearized form it may be shown that:

$$\Delta\phi = \frac{-\Delta s}{R_o \cos\phi_o} \tag{8}$$

where R_o is the radius of curvature of the meniscus surface at the interface.

There are two speeds of concern in the dynamic analysis, the pulling speed V_p and the growth speed V_g. The difference between these speeds determines the velocity of the growth interface in the laboratory frame, and therefore the rate of change of meniscus height. Thus:

$$\dot{s} = \dot{\Delta s} = V_p - V_g \tag{9}$$

Note that in steady state growth $V_p = V_g$

When the meniscus height and meniscus angle differ from their steady state values, the ribbon thickness is changing since the ribbon is then growing with nonvertical faces. By simple geometry it may be seen that for small angles;

$$\dot{t} = 2\, V_g(\Delta\phi) \tag{10}$$

7.5.2 Thermal and Energy Balance Considerations

As discussed previously, the steady state relationship between growth speed and ribbon thickness is determined by the energy balance at the interface. This relationship is reproduced below:

$$V_g \, t^{1/2} = \text{Constant} = C \tag{11}$$

While constant thickness growth requires specific values of meniscus height and meniscus angle any speed-thickness combination which satisfiies eq 11 may constitute an operating point for a dynamic analysis.

Eq 11 may be linearized around an operating point and eq 8 - 11 may be combined to yield the following second order differential equations with ribbon thickness and meniscus height as the dependant systems variables and pulling speed as the externally imposed forcing function.

$$\ddot{\Delta t} + \frac{V_{po}^{\,2}}{R_o \cos \phi_o \, t_o} \dot{\Delta t} = \frac{-2V_{po}}{R_o \cos \phi_o} \Delta V_p \tag{12}$$

$$\ddot{\Delta s} + \frac{V_{po}^{\,2}}{R_o \cos \phi_o t_o} \dot{\Delta s} = \dot{\Delta V_p} \tag{13}$$

These equations predict second order behavior for both ribbon thickness and mensicus height with no damping term present. Reference to the complete analysis of Surek et al[26] shows that the absence of damping term is due to the assumption made in this analysis that the heat conducted up the meniscus may be neglected. All other terms are identical.

In response to a step change in pulling speed. Equations 12 and 13 predict a steady state change in ribbon thickness with no steady state change in meniscus height. It is instructive to qualitatively examine the system response to a step decrease in pulling speed with the aid of Figure 24.

The system begins with steady state growth of ribbon of thickness at speed. The pulling speed is then decreased in a stepwise manner. From the steady state relationship eq 11 we know that the final ribbon thickness will be larger than t_o. However, from eq 10, we see that the thickness cannot change instantaneously. Thus, immediately after the step change t and V_g (from eq 11) remain unchanged. While the growth speed has not changed, the pulling speed has decreased, resulting in a downward motion of the growth interface and a decrease in méniscus height results in an increased meniscus angle according to eq 8, and this, finally results in an increasing ribbon thickness according to eq 10.

It is important to note that the meniscus height must keep decreasing until the ribbon thickness passes through the future steady

state thickness corresponding to the new pulling speed. Only then will the meniscus height begin to return to its steady state value of s_o. However, by the time the meniscus height returns to s_o, the ribbon will be too thick, and it will overshoot in accord with the second order behavior embodied in eqs 12 and 13. As these equations show no damping (due to the neglect of heat transport in the meniscus) they predict that this oscillation will continue. The real system, however, is damped and displays very stable behavior

The model presented above must be extended to include the damping term. Further it should be tested by mesurement of ribbon thickness response to sinusoidal changes in pulling speed, of the type performed by Sachs and Surek for the EFG growth process.[27] No such experiments were conducted during this work.

However it is believed that the arguments presented are valid and serve to explain the nature of the "restoring forces" that give the ESR process absolute stability in respose to a perturbation from steady state growth.

CHAPTER 8

PROCESS LIMITS AND FUTURE PERSPECTIVES

8.1 Process Limits

There is no fundamental limitation to the width of ESR growth. Capillary stabilization of the ribbon edges by attachment to strings will function with arbitrarily wide ribbon, as the meniscus in the center of the ribbon is entirely supported by its attachment to the growing crystal. Thus, the steady state meniscus height derived in Chapter 7 is not a function of ribbon width.

As the ribbon width is increased the region of melt over which a certain temperature tolerance must be maintained increases, and hence might define a limit to ribbon width. However, no severe problems have been encountered in the scale up to 10.0 cm width. This experience indicates that no obvious width limit is imposed by the thermal control requirements.

The primary limit to ribbon width will probably be related to issues of material handling and fragility related to thermally induced stresses. As noted earlier, these are severe and urgent problems which also impact the electronic performance of the material.

The limit to growth speed is a function of the rate of heat removal from the ribbon surface and the ribbon thickness, as discussed in Chapter 7. It is possible to enhance the ribbon cooling by blowing gas on it or other means and thereby increase the growth speed. Such methods however, are not practical as they would exacerbate the already severe thermal stress problem.

Another route to higher growth speeds is available. This modification of the ESR technique involves Angled Growth (sometimes called Horizontal Growth [28]). In vertical growth the length of the growth interface is approximately equal to the ribbon thickness. In angled growth, the interface is greatly enlarged by forcing it to assume an acute angle with respect to the growth direction. This enlargement results in higher growth speeds as more area is available for heat extraction. Additionally, the problems of thermal stress may be reduced as the heat is extracted perpendicular to, rather than along the growth direction. However, as the literature reports, angled growth is difficult to maintain, with dendritic structure often the result. Nonetheless, angled growth remains an extremely promising goal for ESR.

8.2 Conclusions and Future Perspectives

This work has introduced a new crystal growth technique for the growth of thin, ribbon crystals directly from the melt surface. The most important operating feature of this method is that it allows growth over a wide range of melt temperature, on the order of $\pm$ 10°C. This wide control latitude makes the process easy to scale up and promises to allow the process to mature from a laboratory stage to a true manufacturing process. The rapid and timely progress of the technique from the growth of tin ribbon, through the growth of 2.5cm and 5.6cm wide silicon ribbon, to the current status of 10.0cm wide silicon growth, demonstrates the potential of the ESR technique. The photovoltaic quality of ESR has been shown to be good, with the fabrication of 14% efficient solar cells.

This performance is comparable to that achieved by some of the more mature casting and ribbon growth methods. The factors limiting ESR performance are understood and are not considered a fundamental limitation of the process.

The next step in ESR development will be to implement a melt replenishment system and achieve continuous runs of several days duration. Subsequent to that, attention will turn to increasing the throughput of ESR either by angled growth as discussed above, or by the growth of multiple ribbons from the same melt. Stress reduction and the improvement of the electronic performance of the material are continuing goals.

The field of photovoltaics has the potential for great contribution and excitement, but its future is extremely uncertain and to large measure depends on technological progress. There are currently dozens of firms involved in photovoltaic research on many different fronts. Research areas include ingot growth, ribbon growth, amorphous silicon, gallium arsenide thin films, cadmium telluride thin films and many others. At this stage it is difficult to predict which technique or techniques will mature to a low cost manufacturing technology, as all have advantages and disadvantages. However, it is clear that ribbon growth is a leading candidate, and that ESR has great promise for the future.

APPENDIX A

DEMONSTRATION OF ESR USING TIN AS A MODEL MATERIAL

Edge Stabilized Ribbon Growth was first demonstrated by growing 2.5 cm wide Tin ribbon. Tin was selected primarily because the low melting point (230^{o}C) allowed for the rapid construction of experimental apparatus. Tin ribbons 0.5 meters long and 2.5 cm wide were grown at typical speeds of 25 cm/min. Pretinned nickel wire of 0.018 cm diameter were used as the edge supporting string. These were introduced through the melt surface and passed around a pulley submerged in the melt, then up to the growth region.

The low temperature of tin growth did not allow for radiative cooling and it was therefore necessary to blow gas on the ribbon to extract heat. Ribbons of thickness from 0.05cm to as thin as 5 microns were grown depending on the pulling speed and gas flow rate. Figures 25 and 26 below shows the apparatus used for tin growth and some of the ribbons produced. The ribbons have been etched to reveal the grain structure as is evident in the photograph.

Figure 25. 2.5 cm wide ESR tin ribbons.

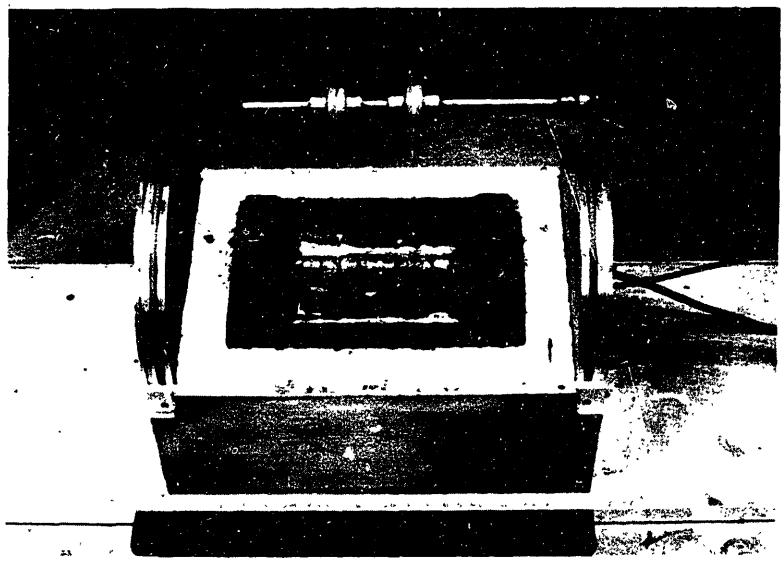

Figure 26. Growth apparatus for tin ESR.

APPENDIX B

STRING MATERIAL THERMAL EXPANSION MEASUREMENT

The degree of thermal expansion mismatch between the string material and the silicon ribbon is a critical concern in selecting a string material. Unfortunately, manufacturer's data is very incomplete on this subject. When any information at all is available, it is usually in the form of a single integrated expansion coefficient from room temperature to some intermediate temperature such as 800 or 1000°C. Thus it became necessary to construct an apparatus capable of measuring the expansion coefficients of string materials through the full range of temperature of interest, up to 1500°C.

Figure 27 presents a schematic drawing of the apparatus built for this purpose. It consists of a self-resistance heated tube supported at either end by the current leads themselves. The tube is surrounded by a silica/alumina type insulation jacket and enveloped by a tubular shell which is entirely purged by argon. The string under test is passed through the center of the self-heated tube and through both end caps. At one end it is anchored to the base of the unit, while the other end passes around the pulley and is then attached to the core of an LVDT. The core of the LVDT provides approximately 5 grams of loading along the fiber, and the LVDT itself provides electrical output proportional to the elongation of the string material. A pure platinum wire is passed through the center of the self-heated tube and isolated from the string

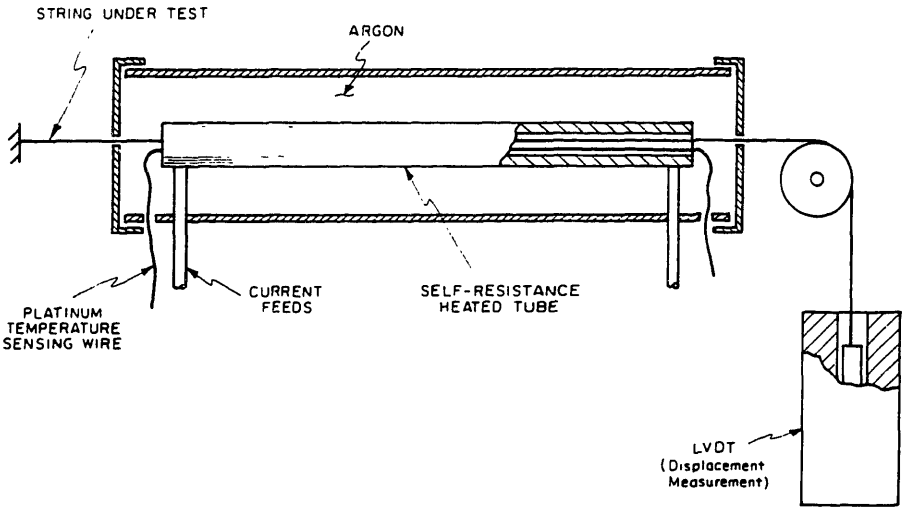

Figure 27. Schematic of apparatus for measurement of the thermal expansion coefficients of string materials.

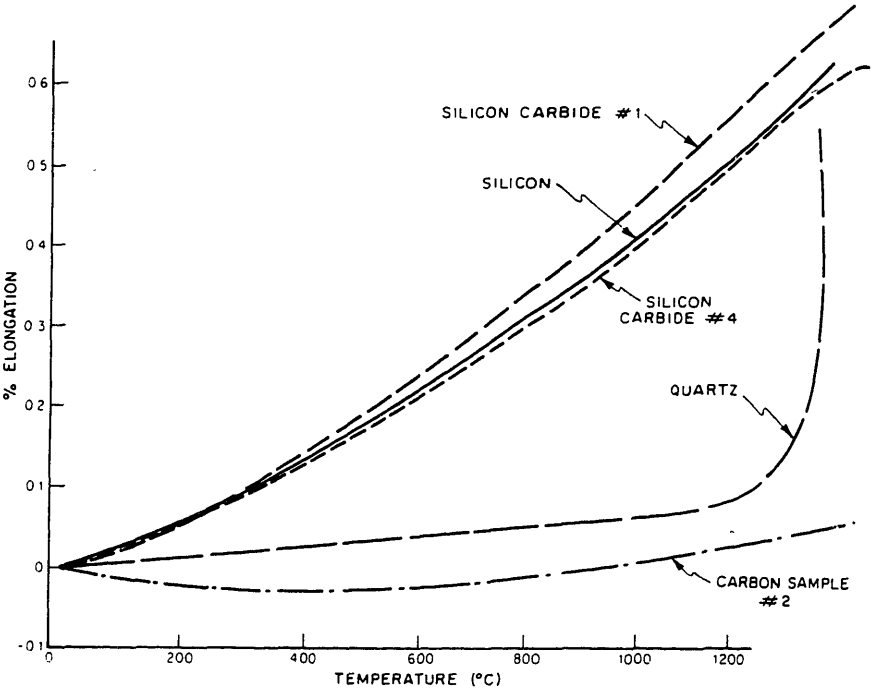

Figure 28. Thermal expansion data of various string materials. The silicon line is taken from the literature[28] Note, the temperature scale is nonlinear; as recorded from a platinum sensor.

and the tube by a small thin-walled alumina tube. The platinum wire is used as a resistance/temperature detector by passing a constant current through it from a current source and measuring the voltage across it. By this technique, an integrated temperature is measured along the entire gauge length involved rather than simply measuring the temperature at a specific point as a thermocouple would do. As the expansion of the string under test in fact responds to this integrated temperature rather than temperature at a specific point, this is felt to be the optimal way to measure temperature in this system.

The electrical outputs of the platinum temperature detector and the LVDT extension measurement are then plotted against each other on an X-Y recorder, thus providing a direct expansion versus temperature curve. In this manner, data may be taken while temperature is increasing, decreasing, or cycling, or the equipment may be used while holding temperature constant in order to examine the creep behavior of a string material under load.

Figure 28 presents a composite of expansion data taken on several string materials. The data presented for silicon is taken from the Thermophysical Properties of Matter by Touloukian.[29] First, note that carbon sample #1 actually displays a negative coefficient of up to approximately 400^{o}C as is typical for graphite multifilament materials. The quartz sample displays a very low expansion which is, of course, just due to viscious flow of the quartz elevated temperature. Most importantly, however, is the expansion data corresponding to the two silicon carbide materials which is fairly close to that of silicon.

Silicon carbide sample #1 displayed especially stable and repeatable measurement with an expansion coefficient slightly greater than that of silicon. On the other hand, silicon carbide sample #4 is quite remarkably close in expansion coefficient to the published data for silicon. Thus we see that candidate string materials are available which display expansion coefficients over an extremely wide range of choice, with several good candidates for expansion matching.

In interpreting the data of Figure 28, it is important to note that the abcissa represents the temperature measurement directly from the platinum sensor and is, therefore, a non-linear scale as indicated by the graduations. Hence, even a constant expansion coefficient would appear on such a graph as a curve with a concave upward shape. For reference, however, comparison of a set of such curves with the data for silicon shows that, in fact, the silicon data does represent an expansion coefficient which increases with temperature.

The data taken with this expansion measurement apparatus has proven extremely reliable with excellent repeatability from one measurement to the next.

APPENDIX C

STEADY STATE MENISCUS HEIGHT

The steady state meniscus height may be derived by integration of the governing differential equation. This equation may be derived by substitution into the Laplace equation (eq. 1, Chapter 7), of the classical expression for the curvature of a plane curve. Alternatively, the governing equation may be derived by examining the vertical force balance on a differential meniscus element as shown in Figure 29 below. The coordinate system is that of Figure 22 where x is the horizontal distance from the ribbon surface and z is the vertical distance from the melt surface.

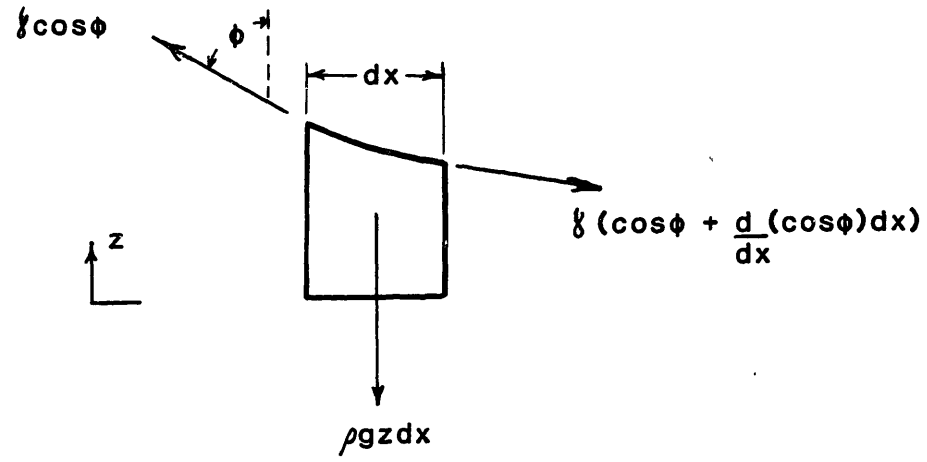

Figure 29. Differential meniscus element.

For this meniscus element, equilibrium gives:

$$-\gamma \frac{d(\cos\phi)}{dx} = \rho g z \qquad (14)$$

By differentiation, use of the chain rule, and noting that $\tan\phi = \frac{dx}{dz}$ it may be shown that;

$$-\gamma \cos\phi \, d\phi = \rho g z dz \qquad (15)$$

This equation may be integrated to yield;

$$z\Big|_{x=\bar{o}} = \left[\frac{2\gamma}{\rho g}(1-\sin\phi_o)\right]^{1/2}$$

where ϕ_o is the value of the meniscus angle required for constant thickness growth.

This is the expression presented as equation 2 of Chapter 7.

APPENDIX D

SPEED-THICKNESS RELATIONSHIP; NEGLECTING HEAT TRANSPORT IN THE MENISCUS

In deriving the steady state speed-thickness relationship in Chapter 7, the contribution of the meniscus heat transport term was neglected as compared with the heat of fusion generated and the ribbon heat transport term. This assumption is supported by a broad base of experience with ESR growth where melt temperature changes made during the growth were observed to have "little" impact on the growth. Equation 3 which describes the interface heat balance is reproduced below for convenience:

$$Q_{men} + Q_{fusion} = Q_{rib} \qquad (3)$$

In order to quantify the relative magnitudes of the terms in eq. 3 an experiment was performed in which ribbon was grown at constant velocity and the melt temperature was changed during growth. The average ribbon thickness was determined by weighing before and after the temperature change. The results are tabulated below, where ΔT is the temperature difference between the bulk of the melt and the melting point;

Table 2. Thickness Change due to Temperature Change

V_g (cm/sec)	ΔT (^{o}C)	Average Thickness (cm)
.056	6.25	.022
.056	13.75	.018

From this data the magnitudes of the three terms of eq 3 may be calculated by assuming specific functional forms for the terms. The forms for Q_{fusion} and Q_{rib} are given by eqs. 4 and 6, respectively. The following form is assumed for Q_{men};

$$Q_{men} = C_2 \Delta T \tag{14}$$

The constants C_1 and C_2 are calculated with the data above and the magnitudes of the terms are found to be:

$$\begin{aligned} Q_{fusion} &= 4.70 \text{ W/cm} \\ Q_{men} &= 0.52 \text{ W/cm} \\ Q_{rib} &= 5.22 \text{ W/cm} \end{aligned} \tag{15}$$

Thus, we see that the heat transport in the meniscus is roughly an order of magnitude lower than the other two terms, and its neglect is justifiable in deriving the speed thickness relationship.

APPENDIX E

INFRA-RED LASER SCANNER

An infra-red laser scanner was constructed as a diagnostic tool to provide a detailed photographic map of the electronic performance of ESR ribbon. As stated in Chapter 6, the photographic output is actually a gray scale representation of the short circuit current generation of the material in response to infra-red light.

The current response to infra-red light is indicative of the quality of the material because of the optical absorption characteristics of silicon. As the wavelengths of incident light increase from the visible to the infra-red, the optical absorption coefficient in silicon decreases, and infra-red light penetrates deep into silicon. If a wavelength shorter than the band edge (photon energies higher than the band gap) is used, electron-hole pairs will be generated deep in the wafer. The current output from the cell is a measure of the number of carriers which reach the front collecting junction, and therefore is a measure of the diffusion length in the material, or the degree of carrier trapping due to crystallographic imperfections. The following relationship between absorption coefficient α, diffusion length L_d, and short circuit current I_{sc} may be derived for the response to infra-red light:[22]

$$I_{sc} = \text{Constant} \frac{\alpha L_d}{1+\alpha L_d} \qquad (16)$$

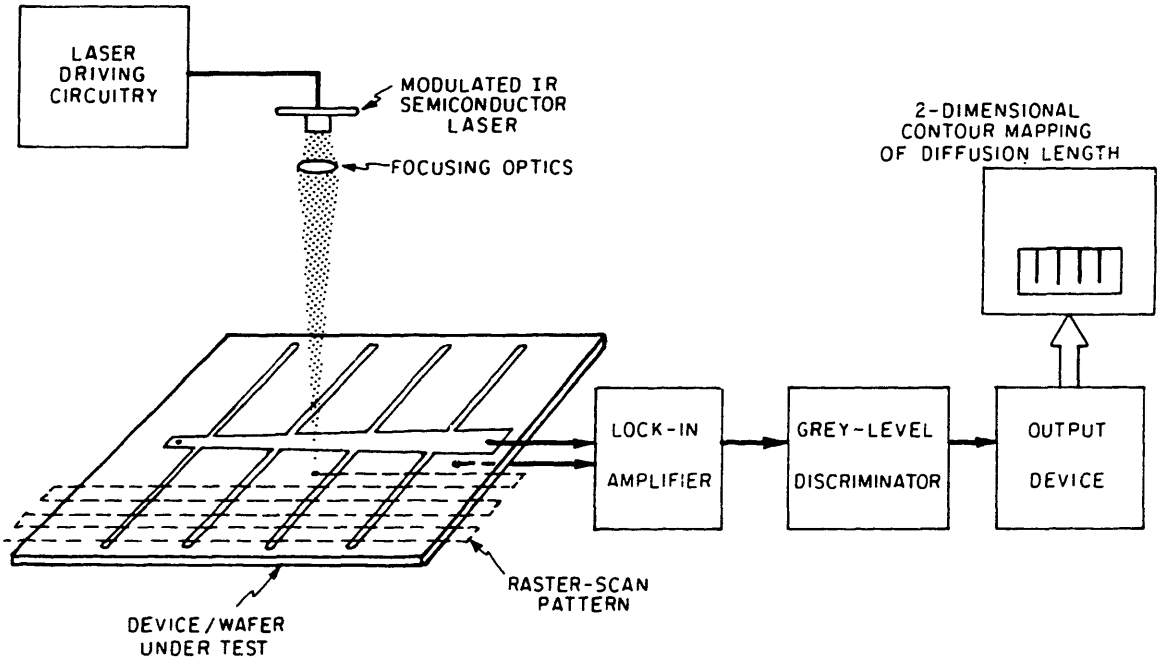

Figure 30. Schematic of infra-red laser scanner.

A schematic drawing of the laser scanner is presented in Figure 30. This machine raster scans the focused beam of a modulated semiconductor laser over the sample being tested. A wavelength of .86 microns was chosen which provides a 1/e penetration depth of approximately 25 microns. This is deep enough to provide good resolution in diffusion length measurement but shallow enough to allow for the testing of thin material. The short circuit current response to the modulated infra-red light is fed to a lock-in amplifier, which is required due to the small signals involved. The signal size is limited to less than 1 microampere because the beam is focused to a small size (approximately 25 microns) to obtain good resolution and the local intensity must be kept low or the carrier traps will saturate and make the measurement invalid.

The lock-in amplifier provides a DC voltage proportional to the device current response. This voltage is the input to six comparators whose set points can be individually selected from ten different preset values which are chosen to correspond to specific diffusion lengths from approximately 5 microns. The comparator outputs are analog summed to produce a signal which has seven discrete levels, including zero. This signal is used to generate a two-dimensional gray scale mapping of the diffusion length, with the grey scale densities corresponding to the six selected diffusion length values.

Examples of the output of the machine are presented in Chapter 6.

APPENDIX F

CURRENT VOLTAGE TESTING OF SOLAR CELLS

Solar cells are tested by measuring their current-voltage (I-V) characteristic under illumination. The I-V plot is the locus of cell response to all possible loading conditions between open circuit and short circuit. A schematic I-V plot is shown in Figure 31.

The intercept with the voltage axis is the open circuit voltage, V_{oc}, which is the maximum voltage the cell is capable of generating. The intercept with the current axis is the short circuit current I_{sc} which is the maximum current the cell is capable of generating. At all points in between, the cell is delivering power to a load. The conversion efficiency of the cell is determined at the peak power point. This point may be found as the point of tangency of the I-V curve to one of a family of constant power hyperbolas as shown in Figure 30. The power generated at this point is $I_{pp}\ V_{pp}$.

The fill factor is defined as the ratio of the areas of the rectangles defined by I_{pp} and V_{pp} to that defined by I_{sc} and V_{oc};

$$FF = \frac{I_{pp} V_{pp}}{I_{sc} V_{oc}}$$

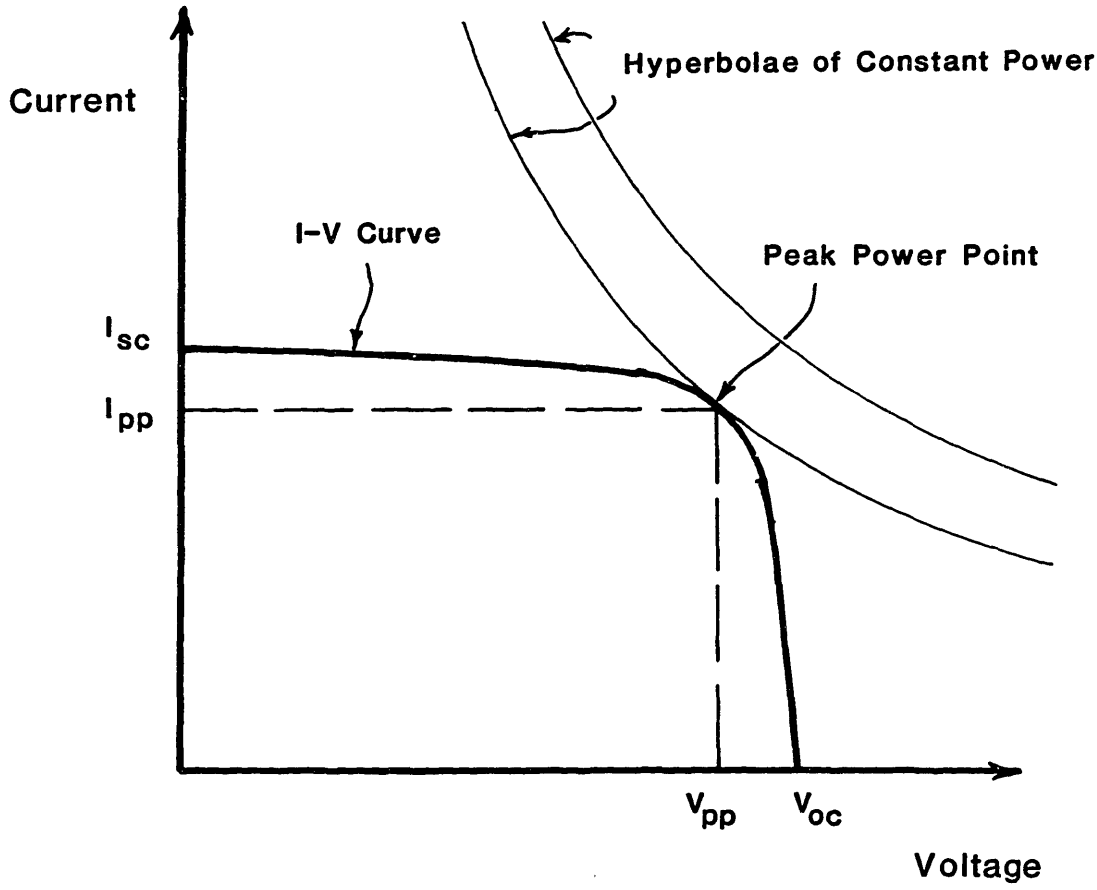

Figure 31. Schematic illustration of the interpretation of an I-V curve.

Thus, the peak power generated may be specified as;

$$\text{Peak Power} = I_{sc} \cdot V_{oc} \cdot FF$$

The results are normalized per unit area by dividing the current values by the cell area to obtain current densities, J, measured in milliamps/cm^2. Thus;

$$\text{Peak Power Density} = J_{sc} \cdot V_{oc} \cdot FF$$

Specification of the three parameters, J_{sc}, V_{oc}, and FF is the preferred characterization of solar cell performance as each has independent meaning. J_{sc} is a measure of the electronic quality of the material and decreases with increasing dislocation density, impurity content, and to a small degree, grain boundaries. V_{oc} if a measure of junction quality. Fill factor is a measure of the "squareness" of the I-V curve, and it decreases with increased cell series resistance and decreased cell shunt resistance. Series resistance results from resistance inherent to a p-n junction, sheet resistance in the top (usually n-type) layer of the cell, and resistance of the metallization

pattern. The slope of the I-V curve at the voltage axis is a measure of series resistance. Shunt resistance is the result of current leakage across the junction. The slope of the I-V curve at the current axis is a measure of shunt resistance.

Finally, the conversion efficiency is calculated from a knowledge of the total incident flux density;

$$\eta = \frac{J_{sc}\ V_{oc}\ FF}{\text{incident flux density}}$$

The standard test conditions of $100mW/cm^2$ total flux make computation of efficiency from J_{sc}, V_{oc} and FF more convenient.

REFERENCES

1. J. Merrigan, "Sunlight to Electricity: Prospects for Solar Energy Conversion by Photovoltaics", MIT Press, 1975

2. J. Fan, "Solar Cells: Plugging into the Sun", Technology Review, Aug/Sept, 1978.

3. J. Fan, "Tandem Solar Cells", Proceedings of SPIE 1983 Technical Symposium East, April, 1983, Vol. 407, to be published.

4. A. Ghosh, C. Fishman, annd T. Feng, "Theory of the Electrical and Photovoltaic Properties of Polycrystalline Silicon", J. Appl. Phys., Vol. 51, Jan 1980.

5. M. Spitzer et al., "Ultra High Efficiency Thin Silicon p-n Junction Solar Cells Using Reflecting Surfaces", Proceedings, 14th IEEE Photovoltaic Specialists Conference.

6. P. Gise, R. Blanchard, "Semiconductor and Integrated Circuit Fabrication Techniques", Prentic Hall, 1979.

7. J. Swartz, T. Surek, and B. Chalmers, "The EFG Process Applied to the Growth of Silicon Ribbons", J Electronic Materials, Vol. 4, No. 2, 1975.

8. J. Kalejs, et al, "Progress in the Growth of Wide Silicon Ribbons by the EFG Technique at High Speed using Multiple Growth Stations", Proceedings, 14th IEEE Photovoltaic Specialists Conference, 1980.

9. R. Seidensticker and R. Hopkins, "Silicon Ribbon Growth by the Dendritic Web Process", Shaped Crystal Growth, North Holland, 1980, page 221.

10. B. Chalmers, et al, "Continuous Silicon Solar Cells", Final Report, NSF Grant GI-37067X, Report NSF/RANN/SE/GI-37067X/FR/1, 1975.

11. M. Harril, et al, "Thermal Analysis of Solidification in Web-Dendritic Ribbon Growth", J. Crystal Growth, Vol 44, 1978.

12. T. Surek, "The Growth of Silicon Sheets for Photovoltaic Applications", Proceedings, Electronic and Optical Properties of Polycrystalline or impure...", Electrochemcial Society, Proceedings Vol. 80-5, 1980.

13. C. Duncan, et al, "Silicon Web Process Development", Annual Report, JPL Contract No. NAS 954654, April, 1979.

14. B. Mackintosh, et al., "Multiple Silicon Ribbon Growth by EFG", Proceedings, 13th IEEE Photovoltaic Specialists Conference.

15. C. Belouet, "The Growth of Polycrystalline Sheets on Carbon Substrates by RAD Process", Proceedings, Electronic and Optical Properties of Polycrystalline or impure...", Electrochemical Society, Proceedings Vol. 80-5, 1980.

16. T. Surek, et al., "Thin-Film Polycrystalline Silicon Solar Cells: Progress and Problems", Proceedings, 15th IEEE Photovoltaic Specialists Conference.

17. J. Zook, "Exploratory Development Program for Silicon-on Ceramic (SOC)", Final Report, SERI Contract No. XS-0-9100-2, Aug. 1982.

18. R. Hopkins, et al., "Effects of Impurities and Processing on Silicon Solar Cells", Phase III Summary and 17th Quarterly Report, JPL Contract No. 954331, Jan 1980.

19. R. Gurtler, "Nature of Thermal Stresses and Potential for Reduced Thermal Buckling of Thin Silicon Ribbon Grown at High Speed", J. Crystal Growth, Vol. 50, 1980.

20. B. Boley and J. Weiner, "Theory of Thermal Stresses", Wiley, 1960.

21. C. Duncan, et al., "Advanced Dendritic Web Growth Development", Quarterly Report, 1981, JPL Contract No. 955843. DOE/JPL 955843/81/2 Dist. Category UC-63.

22. E. Stokes and T. Chu, "Diffusion Lengths on Solar Cells from Short-Circuit Current Measurements", Applied Phys. Letters, Vol. 30, No. 8, 1977.

23. N. Phuoc, and E. Fabre, "Transport Properties in 100mm CZ Silicon", Proceedings 14th IEEE Photovoltaic Specialists Conference.

24. M. Jenkins, "A New Prefferential Etch for Defects in Silicon Crystals", J. Electrochem. Soc. Vol 124, No. 5, 1977.

25. E. Matijevic, "Surface and Colloid Science", Vol. 1, Wiley, 1969.

26. T. Surek, S. Coriel, and B. Chalmers, J. Crystal Growth, Vol. 50, 1980, page 21.

27. E. Sachs and T. Surek, "Dynamics and Control of Meniscus Height in Ribbon Growth by the EFG Method", Shaped Crystal Growth, North Holland, 1980,, page 114.

28. B. Kudo, "Improvements in the Horizontal Ribbon Growth Technique for Single Crystal Silicon", Shaped Crystal Growth, North Holland, 1980, page 247.

29. Y. Touloukian, "Thermal Expansion, Nonmetallic Solids", Thermophysical Properties of Matter, Vol. 13, IFI/Plenum.